UNIVERSITY OF NAPLES FEDERICO II

DOCTORATE IN
MOLECULAR MEDICINE AND MEDICAL BIOTECHNOLOGY

XXXIII CYCLE

Barbara Eleni Rosato

Unraveling the molecular basis of iron overload in rare hereditary anemias: Dehydrated hereditary stomatocytosis and Congenital dyserythropoietic anemia type II

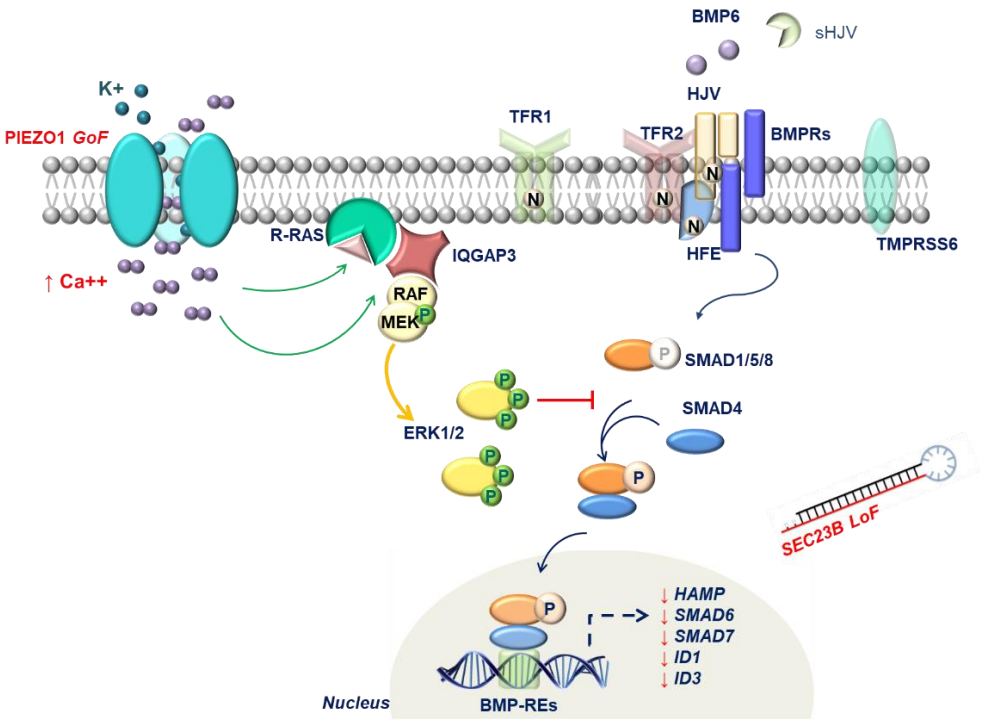

Year 2021

UNIVERSITY OF NAPLES FEDERICO II

DOCTORATE IN
MOLECULAR MEDICINE AND MEDICAL BIOTECHNOLOGY

XXXIII CYCLE

Unraveling the molecular basis of iron overload in rare hereditary anemias: Dehydrated hereditary stomatocytosis and Congenital dyserythropoietic anemia type II

Tutor
Prof. Achille Iolascon

Co-Tutor
Dr. Immacolata Andolfo

Candidate
Barbara Eleni Rosato

Year 2021

Table of contents.

List of abbreviations.

BM: Bone marrow

BMPs: Bone morphogenetic proteins

CDA: congenital dyserythropoietic anemia

CED: C-terminal extracellular domain

COP: Coat protein component

CTD: C-terminal domain

CTR: control

DHS: Dehydrated hereditary stomatocytosis

EPO: Erythropoietin

ERFE: Erythroferrone

FT: Ferritin

FTH: Ferritin heavy chain

FTL Ferritin light chain

GAP: GTPase activating protein

GEF: Guanine exchange factor

GoF: Gain of function

Hb: Hemoglobin

HC: healthy controls

HHA: Hereditary hemolytic anemia

HJV: Hemojuvelin

sHJV: soluble Hemojuvelin

ICE: Inference of CRISPR edits

ID1: Inhibitor of DNA binding 1

LoF: Loss of function

KI: Knock In

MAPK: Mitogen activated protein kinase

MCH(C): mean corpuscular hemoglobin (concentration)

MCV: Mean corpuscular volume

NT: untreated

PKC: Protein kinase C

RBC: Red blood cell

SMAD: small mother against decapentaplegic

I-SMAD: Inhibitory SMAD

R-SMAD: Receptor-activated SMAD

Sh: Small hairpin

Tf: Transferrin

TFR: Transferrin receptor

Abstract

Hereditary anemias are a large group of disorders caused by alterations in genes involved in hemoglobin production, erythropoiesis and red cell structure and metabolism. Among them we focused on: Dehydrated hereditary stomatocytosis (DHS) and congenital dyserythropoietic anemia type II (CDAII). DHS is an autosomal dominant anemia characterized by altered intracellular cation content and cell volume alterations caused by gain of function mutations in *PIEZO1*, a mechanoreceptor activated by various types of mechanical stimuli. CDAII is an autosomal recessive anemia characterized by the impairment of erythroid differentiation and ineffective erythropoiesis. The causative gene of this condition, *SEC23B*, encodes for the homonymous member of the COPII complex, involved in the secretory pathway of eukaryotic cell and that mediates anterograde transport of correctly folded cargo from the endoplasmic reticulum toward the Golgi apparatus. Although patients affected by DHS and CDAII exhibit different phenotypes, they share the strong tendency to hepatic iron overload that represents the most harmful complication in both conditions. Iron overload in DHS patients has already reported to be independent from the degree of anemia, as confirmed by plasma levels of ERFE, the only known erythroid regulator of *HAMP* gene expression. Intriguingly, despite the dyserythropoietic component, we observed that ERFE concentration was almost unvaried in CDAII patients with mild anemia compared to more severely affected patients. These findings suggested that a specific involvement of the two genes at hepatic level could determine the iron overload. We demonstrated that their alteration accounts for a deregulation of BMP/SMAD pathway although through different mechanisms. Particularly, in *PIEZO1* mutated cells (both transient overexpressing model and engineered cells) the increased intracellular calcium concentration leads to deregulation of MAP Kinase pathway that in turns regulates the SMADs expression (at both protein and mRNA levels) resulting in *HAMP* suppression. As proof of the specific PIEZO1 involvement, the selective inhibition of the mechanoreceptor

by GsMTx-4, completely rescued the cellular phenotype observed, restoring the *HAMP* gene transcription. On the other hand, we demonstrated that *SEC23B* loss of function at hepatic level altered the glycosylation, as already found in erythrocytes, of membrane proteins involved in BMP/SMADs pathway activation. Cells silenced for *SEC23B* showed a reduced ability to sense BMP-6 mediated stimulus leading to a reduced expression of hepcidin. Understanding the molecular mechanism that underlie hepatic iron overload will be useful to draw up new therapeutic options for these patients.

1. Background

1.1. Hereditary hemolytic anemias

Hereditary anemias are a large group of diseases caused by mutations in genes involved in hemoglobin production, erythropoiesis, or red blood cell structure and metabolism.

These disorders can be classified in:

I. Hemolytic anemias due to red cell membrane defects (e.g. hereditary spherocytosis, elliptocytosis, hereditary stomatocytosis);(Iolascon, Andolfo, and Russo 2019)

II. Hemolytic anemias due to enzymatic defects (e.g.Glucose-6-phosphate dehydrogenase (G6PD) deficiency, Pyruvate kinase (PK) deficiency);(Grace and Glader 2018)

III. Microcytic anemias due to iron metabolism defects (e.g. iron-refractory iron deficiency anemia (IRIDA), and sideroblastic anemias);(Shokrgozar and Golafshan 2019)

IV. Anemias due to ineffective erythropoiesis (e.g. congenital dyserythropoietic anemias (CDAs). (Iolascon, Andolfo, and Russo 2020)

This thesis project will be focused on the first and fourth groups, particularly on dehydrated hereditary stomatocytosis DHS (I) and CDAs (IV)

1.2. Hemolytic anemias due to red cell membrane defects

Red blood cell (RBC) membrane contains more than 50 trans-membrane proteins and 10 skeletal proteins that interact with each other, and that are responsible for the antigenic proprieties, the transport function, and the mechanical proprieties of the red cell membrane. (Figure 1.1) The specific structural organization of various membrane components is responsible for the

unique features of deformability and mechanical stability of the membrane that are necessary for RBC physiologic function during its long-life span of 120 days. Modulation of erythrocyte shape play a major role in its ability to circulate through micro vessels and splenic slits. It is facilitated by its high membrane surface: volume ratio, the movement of monovalent ions through the activity of different transporters or channels and hemoglobin content. Andolfo et al. (2016); (Badens and Guizouarn 2016) The RBC membrane is one of the best-known membranes in terms of structure, function, and genetic disorders. The disorders associated with defects in the membrane of the RBC comprise a heterogeneous group of inherited diseases affecting membrane proteins or proteins of the cytoskeleton of the RBC. This results in reduced deformability, half-life, and premature removal of erythrocytes from circle. (Andolfo, Russo et al, 2014.) Membrane disorders can be classified into two main subgroups: 1) structural defects, and 2) altered permeability of the RBC membrane. The first subgroup comprises: Hereditary Spherocytosis (HS), Hereditary Elliptocytosis (HE), hereditary pyropoikilocytosis (HPP), and Southeast Asian ovalocytosis (SAO); the second subgroup contains: dehydrated hereditary stomatocytosis (DHS), overhydrated hereditary stomatocytosis (OHS), familial pseudohyperkalemia (FP), and cryohydrocytosis (CHC). The molecular bases of the major hemolytic anemias due to RBC membrane defects have been currently defined. Up to now, 15 different types of anemias due to RBC membrane defects are currently included in the Online Mendelian Inheritance in Man (OMIM) compendium of human genes and genetic phenotypes although the gene mutations identified refer only to a restricted number of patients (Andolfo et al. 2016)

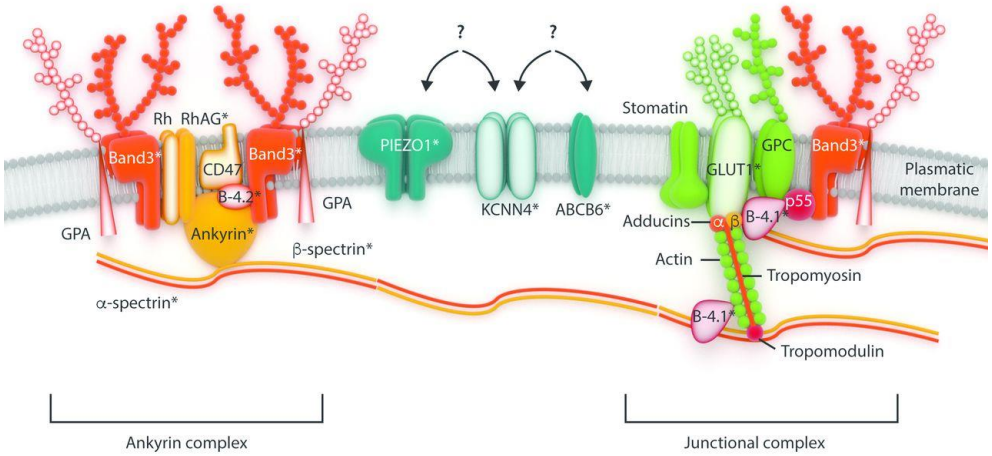

Figure 1.1 Schematic representation of RBC membrane proteins. RBCs membrane proteins pass through the double phospholipid layer. It is possible to distinguish transporters as PIEZO1 and KCNN4, structural proteins as Band3 (an anion exchanger which can be described as the most abundant protein in RBC membrane), Glycophorin C and RhAG. Structural proteins link the double phospholipid layer to cytoskeleton proteins (specially Spectrin α- e β) through proteins like Ankyrin and Protein 4.1. Modified from Andolfo et al 2016.

1.3. Dehydrated Hereditary Stomatocytosis

Regarding disorders associated with membrane transport defects, two distinct phenotypes have been identified: Dehydrated hereditary stomatocytosis (or xerocytosis) and overhydrated hereditary stomatocytosis. (Delaunay 2004) Both exhibit a cation leak to the univalent cation Na+ and K+ resulting in cell volume alterations and altered intracellular cation content. The inheritance of both the conditions is autosomal dominant. The phenotype can vary from asymptomatic to severe hemolytic form. (Da Costa et al. 2013) DHS can be diagnosed alone or frequently as part of a pleiotropic syndrome in association with pseudohyperkalemia and/or perinatal edema. (Grootenboer et al. 2000) It consists of a usually compensated hemolysis, associated with moderate splenomegaly. The reticulocyte count is elevated, and red cell mean corpuscular volume (MCV) is slightly increased. The cation leak is mild in DHS red cells; however, cells preferentially lose K+ ions causing dehydration and leading to an increased MCHC. (Bruce 2009) Its incidence is about 1:8,000 live births in a recent estimation from USA population. (Kaufman et al. 2018)

As a rough estimation, it is ten to twenty-fold less frequent than spherocytosis, with which it may still be confused and for this reason the condition may be overlooked for years or decades. The salient features of stomatocytosis is the presence of the so-called “stomatocytes” on blood smears, erythrocyte containing a linear unstained area across their center, instead of the normal circular area of pallor. Nevertheless, stomatocytes are rare and ill-formed except for some cases. (Delaunay 2004) (Figure 1.2A) The “gold standard” for the diagnosis of DHS is the osmotic gradient ektacytometry which shows a specific curve. (Figure 1.2B). The ektacytometer is a viscometer, in which the deformation of RBCs, at defined values of applied shear stress, is monitored as a continuous function of suspending medium osmolarity. Three distinct parameters are considered: i) the “Omin” point, which corresponds to the osmolarity at which 50% of the red cells are lysed in the classical osmotic fragility test; ii) the maximal deformability index (“DImax”) value, which represents the maximal cellular deformability of the red cell population; iii) the O' or hyper point, which corresponds to the osmolarity at DImax/2, which reflects the hydration status of the red cells. (Zaninoni et al. 2018) The thrombotic tendency in hereditary stomatocytosis is strikingly severe so splenectomy is banned. As reported in several studies (Iolascon et al. 2017), the procedure is of limited hematological benefit and seems to carry a significant risk of morbidity and mortality in later life. Thrombosis is a well-described complication after splenectomy, particularly when removal of the spleen does not abrogate hemolysis. Several factors may be involved, including platelet aggregation, decrease in nitric oxide level, high level of circulating microparticles, high rate of phosphatidylserine-expressing red cells and increased reticulocyte adherence. (Cappellini et al. 2005; Gallagher et al. 2003) The candidate gene locus was first localized at 16q23-24. (Carella et al. 1998; Grootenboer et al. 2000) and several years later, *PIEZO1* was identified as the first causative gene of DHS by exome sequencing. (Andolfo et al. 2013; Zarychanski et al. 2012) PIEZO1 encodes a mechanoreceptor, an ion

channel activated by pressure whose expression is not limited to erythrocyte (see below). (Coste et al. 2015) Recently, a second candidate gene, *KCNN4*, has been identified as causative of a different form of DHS named DHS2 or Gardos Channelopathy. (Rapetti-Mauss et al. 2017) The two forms of DHS showed very similar phenotype even if some differences can be observed. Recent in vitro studies showed that both DHS1 and DHS2 share a common pathophysiology leading to red cell dehydration. (Rapetti-Mauss et al. 2015; Rapetti-Mauss et al. 2017). Nevertheless, regarding hematologic parameters for each genotype, DHS2 patients were characterized by lower hemoglobin level, reticulocyte count and mean corpuscular hemoglobin concentration than DHS1 cases. (Picard et al. 2019) A relevant clinical implication of DHS patients is the iron overloading capacity. Several patients in treatment for iron overload have revealed an undiagnosed stomatocytosis. Although the mechanism responsible for the accumulation of iron in patients with DHS is still unclear, it is known that patients have considerable deposits of iron in the heart, liver and pancreas, leading to the same clinical manifestations as those found in patients with thalassemia and sickle cell anemia with secondary hemochromatosis. (Assis et al. 2013) Severe iron overload is frequent in DHS. In the last years the well-compensated hemolysis and the little transfusion requirement guided the idea that iron overload was completely independent from the erythroid involvement. (Orvain et al. 2018) Only recently, the PIEZO1 activation was reported to have a role in erythroid differentiation, particularly impairing proliferation and differentiation of erythroid progenitors through transcriptional regulation. (Caulier et al. 2020) Indeed, hyperferritinemia, was frequently at the front line of the diagnosis and as it is much more frequent in DHS than in other hemolytic anemias as spherocytosis. (Barcellini and Fattizzo 2015; Mariani et al. 2008) A recently genotype-phenotype correlation in patients with hereditary stomatocytosis revealed that PIEZO1 and KCNN4 patients showed impairment of the iron balance as ferritin levels and ferritin levels normalized on the age. Particularly mean serum ferritin dosage attested a tendency to iron

overload in both DHS1 and DHS2 although the ferritin/age ratio reached highest values in DHS1 than DHS2. Moreover, PIEZO1 transfused patients (33.3%) showed average ferritin of 585.3 ng/mL *vs* an average of 672.3 ng/mL of non-transfused patients, suggesting that the iron overload is independent from the transfusion rate in these subjects. (Andolfo, Russo, et al. 2018) As previously demonstrated, PIEZO1 mutations are associated to severe iron loading condition, assuming a crucial role of the mechanoreceptor in iron metabolism regulation although molecular bases are still not clear. In some cases, HFE mutations have been reported to worsen iron overload in DHS (Syfuss et al. 2006). Alternative mechanisms of increased iron uptake may be involved, including chronic hypoxia, increased erythroferrone secretion, and erythroblast proliferation possibly associated with some inefficient erythropoiesis. Alternatively, expression of a mutated PIEZO1 or Gardos protein at the cell surface could directly deregulate hepcidin expression in liver cells or drive iron entry through the gut. (Picard et al. 2019)

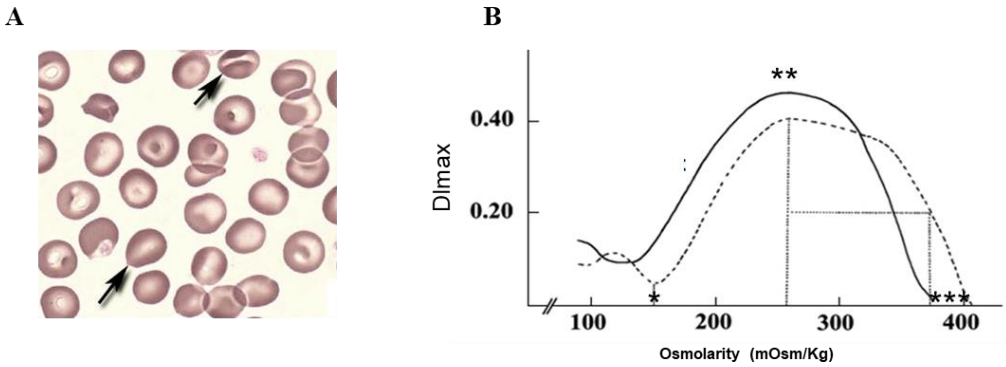

Figure 1.2. **Clinical feature of DHS. A.** Stomatocytes are highlighted on a blood smear (black arrow) **B.** Osmotic gradient ektacytometry on a DHS patient (continuous curve), left-shifted respect of healthy control (dashed curve). Parameters of interests are signed: ****Dlmax** (maximal deformability index)*; ****0min** (ipo-osmotic point)*; ****** 0'** (iper- osmotic point).* Modified from Andolfo et al., 2016.

1.4. *PIEZO1*: the first causative gene of dehydrated hereditary Stomatocytosis

PIEZO proteins are evolutionarily conserved and functionally diverse mechanosensitive cation channels. Their role in mechanotransduction in mammalian cells, as the localization on plasma membrane has been clarified by Coste and colleagues in 2010. PIEZO1 has several roles in multiple physiological processes, including cell migration and differentiation, sensing shear stress of blood flow for proper blood vessel development, and particularly it regulates red blood cell function in terms of development/homeostasis, volume homeostasis, and deformability. (Faucherre et al. 2014)

PIEZO1 forms a trimeric propeller-like structure of about 900 kilodalton (Figure 1.3), with the extracellular domains and a central cap. The transmembrane region has 14 apparently resolved segments per subunit. These segments form three peripheral wings and a central pore that encloses a potential ion-conducting pore. Each monomer has three functional different components. Firstly the transmembrane skeleton containing 14 transmembrane segments. A topological prediction model suggests that residues from 2210 to 2457 (termed the C-terminal extracellular domain, CED) constitute a large extracellular loop (Figure 1.3). Secondarily, the ion-conducting pore represents the center of the PIEZO1 channel within the membrane. It consists of six transmembrane helices and includes the inner and outer helix, the CED and the C-terminal domain. Finally, the flexible blades represents the potential force sensor. (Lin et al. 2019) Several mutations have been reported for PIEZO1, mostly missense. The single point mutations slow the inactivation and introduce a long latency followed by activation of groups of channels. The mechanism through which these changes lead to DHS might concern the alteration of the mechanical sensitivity of the channel and the change of ions flux that accompanies mechanical stress, particularly as the RBC pass through capillaries. The slowing of the inactivation may be more important than the

channel sensitivity to stress. A second, nonexclusive possibility is that mutant channels do not activate when needed during capillary transit in different kind of cells. (Bae et al. 2013) Another important feature of PIEZO1 that may contribute to the clinical presentation is its ability to pass calcium.(Glogowska et al. 2017)

The chemical activation of the channel was demonstrated to be related to the activation of intracellular Ca^{2+} dependent signal transduction as NFATs, Calcineurin, MAPK, and calcium dependent PKCs. (Lanuti et al. 2006; von Lindern et al. 2000) In several cases, this activation was associated to modification of membrane integrin mainly affecting the adhesive properties of, endothelial cells (Chen et al. 2018) epithelial cells (McHugh et al. 2012) and erythroblasts.

In particular, activation of downstream Ca2+-mediators Calpain and PKC, results in inside-out activation of integrins leading to increased adhesive properties of erythroblasts. (Aglialoro et al. 2020). Mutational analysis confirmed the link between several different mutations in *PIEZO1* with the pathogenesis of DHS. (Albuisson et al. 2013; Shmukler et al. 2014)

The role of PIEZO1 and the change connected to its mutations have been deeply investigated by the means of electrophysiological and functional studies both *in vitro* and *ex vivo*. Functional studies in *Xenopus* oocytes demonstrated that PIEZO1-WT expression increased 2-electrode voltage clamp current elicited by osmotic swelling, and channel activity in cell-attached patches. The mutation p.R2488Q in PIEZO1 increased hydrostatic pressure-induced currents in on-cell patches of *Xenopus* oocytes, likely reflecting, in part the increased channel open probability (NPo). Oocytes expressing PIEZO1 mutant, p.R2456H, exhibited cell-attached patch currents of elevated single-channel conductance. These properties of oocytes expressing PIEZO1 mutants are consistent with the steady-state elevation of intracellular Na+ and reduction of intracellular K+ that characterize RBCs of DHS patients. (Andolfo et al. 2013) Moreover, a new mutation has been found in two unrelated families. The

mutation consists of a heterozygous in frame duplication of two amino acids, p.E2492_L2493dup located in the C-terminal intracellular domain. Interestingly one of the affected probands showed an additional *in cis* PIEZO1 variant c.5591G>A, p. R1864H that was found to be a *de novo* mutation. Functional studies demonstrated that this missense rare variant accounts for an augmented K+ efflux when co-inherited with the duplication, probably leading in turn to the more severe anemia observed in the affected proband. (Andolfo, Manna, et al. 2018) This finding highlighted the importance to study the effect of multiple modifier PIEZO1 variants on the genotype-phenotype correlation, since it is well-known that a lot of mendelian disorders could be explained with the combinations of multiple disease-causing alleles, or their combination with polymorphic variants.

In 40.9% of cases the mutations localized in the C-terminal regions codifying for the central pore region encompassing CTD (C-terminal extracellular domain), inner helix, CED (extracellular domain), outer helix, responsible of the pore properties (ion conduction and cation selectivity). (Andolfo, Russo, et al. 2018)

Andolfo and colleagues demonstrated that patients showing a more severe phenotype carried mutations in the pore domain of the channel, responsible of the ion passage, while patients showing a less severe phenotype carried mutations in the non-pore domain, responsible for the mechanosensitive properties of the channel. Mutations in the pore domain could be related to severity of the condition, including hemolysis and iron balance, since this domain is responsible for either the ion conduction and cation selectivity or the interaction with other proteins by its cytoplasmic code, and thus it is involved into the intracellular signaling pathways. (Andolfo, Russo, et al. 2018)

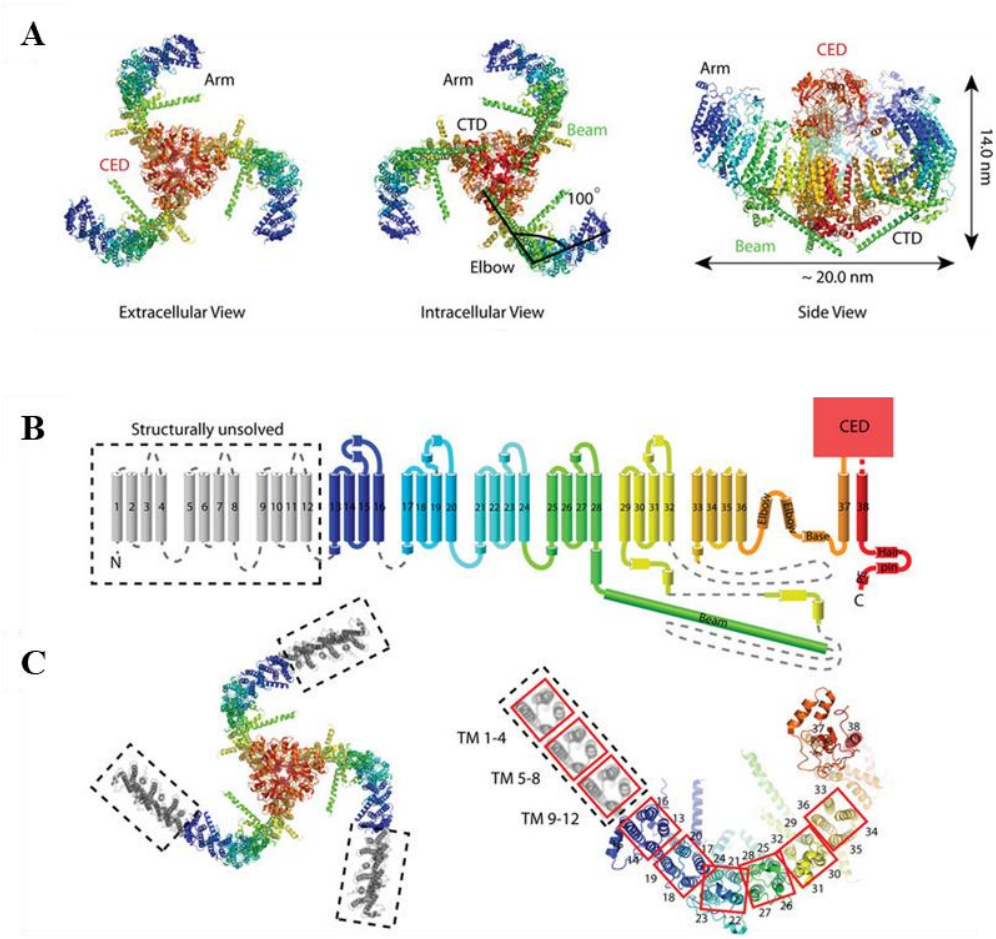

Figure 3: Architecture and topology of the mechanosensitive channel PIEZO1. **A.** Top, bottom, and side views of PIEZO1 in cartoon representation. **B.** Topology of PIEZO1 shown rainbow-colored (with N terminus in blue and C terminus in red), except for the structurally unsolved TM1–TM12 regions (shown in grey). Helices are represented as cylinders, loops as solid lines and unresolved regions as dotted lines. **C**. Top view of transmembrane helices labelled as in the topology. Red squares outline four-transmembrane units that constitute the arm. TM21–TM24 are at the 'elbow' of the arm. The hypothetical position of the unresolved units TM1–TM4, TM5–TM8 and TM9–TM12 are indicated (dashed outline). Modified from (Lin et al. 2019)

1.5. *KCNN4*: the second causative gene of Dehydrated Hereditary Stomatocytosis

KCNN4 channels are prominently expressed in cells of the hematopoietic system and in organs involved in salt and fluid transport, including the colon, lung, and salivary glands. Heterologous expression of KCNN4 produces K^+-selective, Ca^{+2}-activated channels without time or voltage dependence. (Begenisich et al. 2004) Basing on amino acid sequence, the Gardos channel is thought to be a homo-tetramer of six-transmembrane-domain polypeptides. The region between the S5 and S6 membrane domains contains the pore region, analogous to that seen in other K^+ channel with already known structure. (Figure 1.4) KCNN4 was discovered to be involved in the pathogenesis of DHS, according to its role in maintaining the hydration status of RBC as demonstrated using a specific inhibitor, Senicapoc, which reduce erythrocyte dehydration. (Ataga et al. 2011)

Mutational analysis on patients of unrelated families revealed different mutations in *KCNN4* gene; the more frequent and known mutations are p.R352H, (Andolfo et al. 2015; Rapetti-Mauss et al. 2015) and p.V282M. (Glogowska et al. 2015) The residue affected by the first mutation located in a conserved site, involved in the interaction with Calmodulin and responsible for the channel opening and the K^+ efflux (Rapetti-Mauss et al. 2015) instead the V282M residue is modeled near the C-terminal cytoplasmic end of transmembrane span S6 of the pore-forming domain. (Andolfo et al. 2015) Moreover, the ektacytometry profile of V282M mutation is left-shifted to an unusually extreme degree indicating reduced shear-sensitive deformability is consistent with profound red cell dehydration. (Rivera et al. 2017) As in DHS, patients with mutation in the Gardos channel show variability in disease severity. In addition, this point could shed light on PIEZO1 function in erythrocyte, suggesting that PIEZO1 and the Gardos channel might act in the same stretch-induced cation pathway involved in cell volume changes.

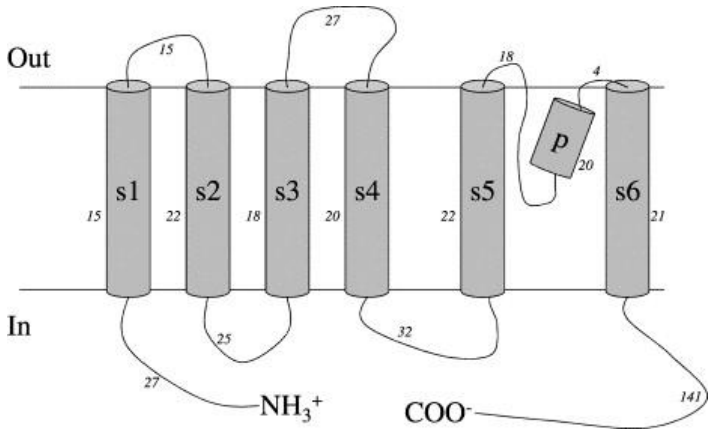

Figure 1.4. Schematic representation of the topology of the monomeric subunit of the Gardos channel in a cell membrane. The s1–s6 regions are the six putative transmembrane domains and 'p' represents the pore-forming region with its selectivity filter. The total number of amino acids is 427 and its molecular mass is 47.8 kDa. It is predicted that the functional channel is a tetramer. Modified from (Maher and Kuchel 2003)

1.6. Congenital dyserythropoietic anemias

The term dyserythropoiesis refers to a condition of abnormal erythropoiesis affecting the differentiation and proliferation pathways of the erythroid lineage with a consequent defective production of RBCs. (Iolascon et al. 2011) Congenital Dyserythropoietic Anemias (CDAs) are hereditary diseases that embrace a highly heterogeneous set of rare or very rare anemias that result from various abnormalities during late stages of erythropoiesis. CDAs can be suspected in the presence of anemia and hemolytic signs, accompanied with reticulocytosis inadequate to the degree of anemia. (Gambale et al. 2016) The bone marrow of CDA patients is always hypercellular, due to an exclusive and pronounced increase of erythroblasts, with erythropoietic/granulopoietic ratio (E:G) of 4 to 10 (normal reference values 0.3 - 1.0). Dyseritropoiesis appears to be a morphological feature common to several conditions, and this could account for the difficulties in diagnosis of CDAs. However, the specific morphological alterations of the erythroid precursors justify the heterogeneity of these disorders. The three classical types of CDAs (types I, II and III) are based on bone marrow morphology. (Iolascon et al. 2013) From the genetic

standpoint, six different types of CDAs are included in OMIM compendium of human genes and genetic phenotypes. In the majority of CDAs, inheritance is autosomal recessive and single cases in one family are mostly identified. Because of the rarity of the disorder and the need to obtain bone marrow specimens for diagnosis, correct diagnosis is often delayed. (Iolascon, Andolfo, and Russo 2020) (Russo et al. 2020). The studies on molecular epidemiology of CDA I and II highlighted the elevated allelic heterogeneity of both conditions as most of the causative variations are inherited as private mutations. (Iolascon, Esposito, and Russo 2012)

1.7. Congenital dyserythropoietic anemia type II

Congenital dyserythropoietic anemia type II (CDA II) is the most common form among CDAs. The main clinical finding to diagnose CDA II is the presence of normocytic anemia of variable degree, with normal or only slightly increased reticulocyte count, but not adequate to the degree of anemia (ineffective erythropoiesis); it is often accompanied with jaundice and splenomegaly due to the hemolytic component. (Iolascon, Andolfo, and Russo 2020) As described, CDA II generally presents mild anemia, but a wide spectrum of clinical presentations can occur, from asymptomatic to severe (Hb range 3.6-16.4 g/dL). Indeed, approximately 10% of cases result symptomless, whereas 20% of patients undergo a regimen of transfusion dependence. (Russo et al. 2014) The bone marrow is hypercellular with distinct erythroid hyperplasia and subsequent increased E:G. The most specific finding is the presence of more than 10% mature binucleated erythroblasts with equal size of two nuclei. The analysis of RBC membrane proteins by sodium dodecyl sulfate polyacrylamide (SDS-PAGE) gel electrophoresis reveals a slighter band size and faster migration of band 3 in most of the CDA II patients (95%) (Figure 1.5A, B). Thus, this biochemical feature represents a specific diagnostic hallmark of the disease. Moreover, the hypoglycosylation of band 3 has been associated to the occurrence of the hemolytic component observed in CDA II

patients by means of increased clusterization of this protein on RBC surface, which in turn leads to IgG binding and phagocytosis of RBCs. (De Franceschi et al. 1998) Both morphological features of the bone marrow and biochemical alterations of RBC membrane proteins can be explained by the mutations in the causative gene *SEC23B* (chr 20p11.23). (Schwarz et al. 2009) Most of CDA II cases show biallelic mutations in *SEC23B* gene, although a subset of patients with an incomplete pattern of inheritance has been identified. More than 80 different mutations in *SEC23B* have been described so far, even if recurrent variants have been also described. Conversely, the presence of two hypomorphic alleles accounting for mild CDA II clinical forms was described. (Russo et al. 2013) Although no direct evidence exists, SEC23B could play an active role in assembly or deconstruction of the midbody, where it was identified in a proteomic screen. (Skop et al. 2004) The multinuclear phenotype could be secondary to the aberrant glycosylation of specific proteins required for cell division, leading to defects in this process. However, it remains to unravel how alterations in a ubiquitous gene can result in clinical manifestations restricted to the erythropoietic tissue. The specificity of the CDA II phenotype seems to be due to the tissue-specific expression of SEC23B during erythroid differentiation. (Schwarz et al. 2009) Alternatively, it could be explained by the presence of erythroid-specific cargoes (such as band 3), which might require high levels and full function of a specific COPII component to be correctly transported (Russo, Esposito, and Iolascon 2013). Iron overload is the most frequent complication of CDAs. It is mainly the result of ineffective erythropoiesis, and it is also linked to both the transfusion regimen and the hemolytic component. (Gambale et al. 2016) Among CDAII patients, ~30% of not transfusion dependent patients show increased ferritinemia (ferritin >300 ng/mL), whereas 17% of them show marked hemosiderosis (ferritin >600 ng/mL). (Iolascon, Andolfo, and Russo 2020) The severe phenotypes can be related to coinheritance of modifier mutations, such as polymorphic variants in the *HFE* gene, which causes hemochromatosis type 2. (Liu et al. 2012) The

mechanism of hepatic iron overload in patient with CDAII has been associated to the reduced expression of the hepatic hormone hepcidin. Some erythroid regulators have been proposed as pathological suppressors of hepcidin, such as growth differentiation factor 15 (GDF15), (Casanovas et al. 2011; Tamary et al. 2008; Tanno et al. 2007) although GDF15 alone does not appear to be necessary for physiological hepcidin suppression. (Casanovas et al. 2013) More recently, erythroferrone (ERFE) has been studied in CDAII patients who showed increased levels of the hormone compared with healthy controls (Russo et al. 2016) Notably, patients with high levels of ERFE also had reduced hemoglobin levels and increased erythropoietin levels compared with patients with lower levels of ERFE. This, in turn, leads to reduced hepcidin and hepcidin-to-ferritin ratio, which results in augmented iron delivery to the erythron. (Russo et al. 2016) Recently, a recurrent low-frequency variant in the ERFE gene was identified (i.e., p.A260S) in 12.5% of CDAII patients with severe phenotypes, using an 81-gene targeted sequencing panel for modifier genes. (Andolfo et al. 2019) The ERFE-A260S variant results in increased levels of ERFE, with subsequent marked impairment of iron regulation pathways at the hepatic level. Functional characterization of ERFE-A260S in the Huh7 hepatic cell system demonstrated its modifier role in iron overload through impairment of the BMP/SMAD pathway, and the consequent reduction in hepcidin expression. This finding confirms the role of ERFE in the development of hepatic iron overload in CDAII, even if other actors might be involved in this scenario to explain the impairment of iron metabolism in these patients. (Andolfo et al. 2019; Russo et al. 2016)

1.8. *SEC23B*: the causative gene of Congenital dyserythropoietic anemia type

SEC23B, the causative gene of CDA II, encodes the cytoplasmic coat protein component (COP) SEC23B, which is involved in the secretory pathway of eukaryotic cells. (Russo, Esposito, and Iolascon 2013; Schwarz et al. 2009) Three well-characterized coat complexes, clathrin, and coat protein complexes I and II (COPI and COPII), have been described; they are multi-subunit complexes that recognize specific protein sorting signals and selectively sort proteins into carrier vesicles. Particularly, SEC23B is involved in COPII recruitment that is initiated by the activation of the small GTPase Sar1 by its Endoplasmic reticulum-localized guanine exchange factor (GEF), Sec12. Sar1 initiates vesicle formation on ER membranes through the exchange of GDP for GTP, which induces tight membrane association of Sar1 and the subsequent recruitment of the heterodimeric complex comprising of Sec23/24 COPII components. (Antonny et al. 2001) Sec23 is a GTPase activating protein (GAP) that stimulates the enzymatic activity of Sar1, whereas Sec24 is the adaptor protein that captures specific cargo into the nascent vesicle. The Sar1-GTP/Sec23/Sec24 ‘‘pre-budding’’ complex in turn recruits the Sec13/Sec31 heterotetramer, which forms the outer layer of the COPII coat, a flexible coat cage that can accommodate various sizes of vesicles, and likely functions to cross-link adjacent prebudding complexes and complete the vesicle biogenesis process (Khoriaty et al. 2014) (Figure 1.6). Sec23b-deficient mice have no apparent anemia phenotype, but they die shortly after birth with degeneration of secretory tissues, including pancreas and salivary glands. The disparate mouse and human phenotypes may result from either residual SEC23B function associated with the hypomorphic mutations found in humans or a species-specific shift in function between the closely related paralogues, SEC23A and SEC23B. Of note, SEC23A and SEC23B are paralogous components of the COPII complex. (Khoriaty et al. 2014) It has been suggested that compensatory expression of SEC23A could ameliorate the effect of

reduced SEC23B expression. (Tao et al. 2012) The pathophysiology study is difficult mainly because of the absence of a reliable animal model. Different models of SEC23B-deficient mice have been generated without reproducing CDA II phenotype. This observation agrees with the compensatory expression of SEC23A that seems to ameliorate the effect of low SEC23B expression alleles in CDA II patients. (Russo, Esposito, and Iolascon 2013) So far, the only reliable in vitro model for CDA II is the *SEC23B*-silencing in K562 cells, which recapitulates the cytokinesis defect, with a significant increase of percentage of binuclearity and an increased size of nuclei in *SEC23B*-silenced cells. (Schwarz et al. 2009)

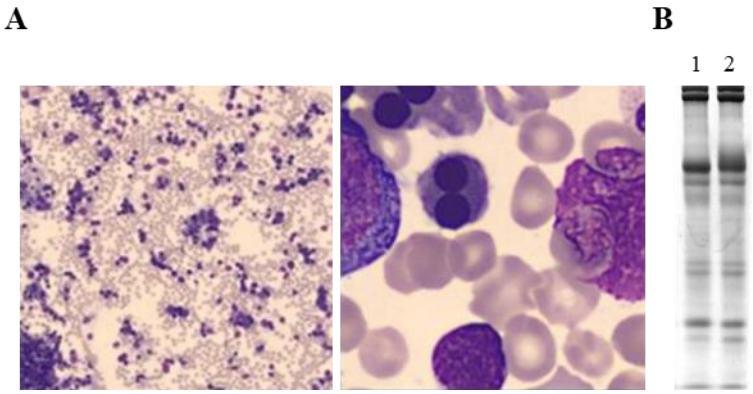

Figure 1.5. Morphological and biochemical features of CDA II. A. CDA II bone marrow at light microscopy highlights erythroid hyperplasia with bi- or multinucleated late erythroid precursors. **B.** Biochemical analysis of RBC membrane proteins from CDA II patient (lane 1) shows the typical hypoglycosylation of Band 3, with an increased anodic mobility on SDS-PAGE compared to healthy control (lane 2).

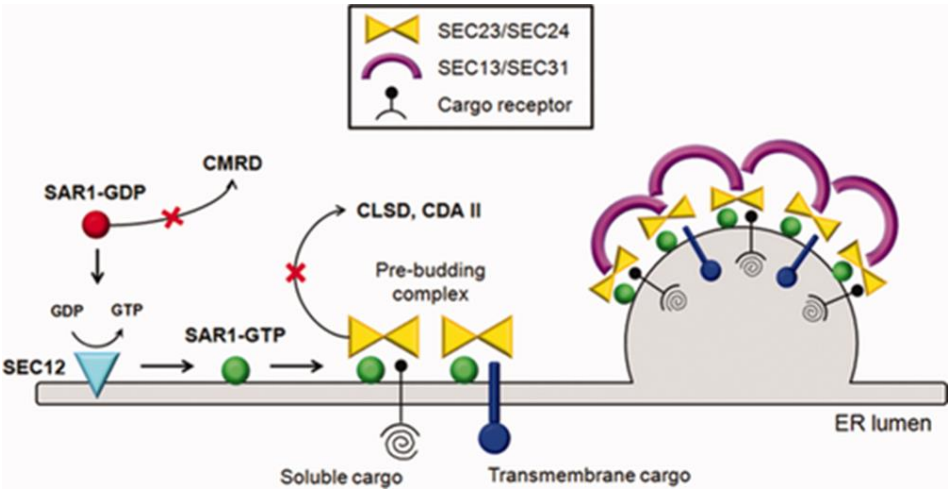

Figure 1.6. Recruitment mechanism of COPII. COPII-coated vesicles form by the sequential binding of Sar1-GTP, the inner complex proteins Sec23- Sec24 and the outer complex components Sec13-Sec31 on the endoplasmic reticulum. The transport of both integral membrane cargo and soluble secretory cargo is shown. Modified from Russo R. et al, 2013.

1.9. Iron metabolism

Iron is, after aluminum, the second most abundant metal on Earth, and is an essential element for all forms of life. Numerous enzymes involved in DNA replication, repair and translation rely on iron, often in the form of iron-sulphur (Fe-S) clusters. The biological activity of iron lies in its efficient electron transferring properties, enabling it to accept or donate electrons while switching between its ferrous bivalent (Fe(II), Fe2+), ferric trivalent (Fe(III), Fe3+) and its ferryl tetravalent (Fe(IV), Fe4+) states. (Crielaard, Lammers, and Rivella 2017) Considering the vital functions of iron in human physiology, systemic or cellular disorders in iron metabolism may have serious consequences. At the systemic level, heme incorporated in hemoglobin and myoglobin accounts for more than half of the approximately four grams of iron present in the human body, and by far the largest share of the total iron turnover is for heme production. Consequently, an insufficient iron supply will lead to a lack of Hb, resulting in iron-deficiency anemia. (Ganz 2013) At the cellular level, the presence of intracellular iron has a strong impact on the

cellular redox status, contributing to oxidative stress in individual cells. (Stadtman 1992) Systemic iron homeostasis comprehends the absorption of dietary iron, the concentration of iron in extracellular fluid and blood plasma, and the release of iron from macrophages involved in recycling and from iron-storing hepatocytes. It now appears that there is a single systemic regulator of iron, the hepatic peptide hormone hepcidin. The hormone controls the concentration of iron in plasma, inhibits the transfer of dietary iron from duodenal enterocytes to plasma, the release of recycled iron from macrophages to plasma, and the release of stored iron from hepatocytes. (Ganz and Nemeth 2012) Cellular iron trafficking can be separated into three processes: intake, utilization, and efflux. (Figure 1.7).

1.9.1. Iron intake

To acquire such high amounts of iron, cells depend on transferrin (Tf). Transferrin is a glycoprotein with two high-affinity sites for FeIII and is necessary for iron circulation avoiding formation of toxic radicals and limiting iron access to invading pathogens, which also require iron. In healthy individuals, Tf is about 30% saturated with iron and is mainly destined to the erythroid marrow. Diferric Transferrin (Tf-Fe2) binds to the high-affinity Transferrin receptor 1 (TFR1, also known as TFRC, CD71) on the surface of developing RBCs. Tf-Fe2/TFR1 complex enters in cells by endocytosis. (Muckenthaler et al. 2017) Iron release from transferrin requires the acidic environment, then the freed metal is then reduced to the ferrous form by STEAP3 (six-transmembrane epithelial antigen of prostate 3) and transported into the cytosol by DMT1 (divalent metal transporter 1). (Ohgami et al. 2005) Transferrin receptor-2 (TFR2) is a type II transmembrane glycoprotein homologous to TFR1. TFR2 has a lower affinity for transferrin and does not significantly contribute to iron import. It serves as a sensor of Tf-saturation. TFR2 is mainly expressed in the liver where it is essential for hepcidin control. It is highly expressed in erythroblasts, where it modulates EPO receptor

signaling possibly to adjust RBC production to Tf-Fe2 availability. (Nai et al. 2015) As a further level of complexity, the TFR2 gene is expressed in immature erythroid cells where it is a component of the erythropoietin receptor (EPO-R) complex. The TFR2-EPOR association is required for the efficient transport of EPOR to the cell surface. All these properties make TFR2 a good candidate as a sensor for iron bound to circulating Tf, measured as transferrin saturation (TSAT). (Pagani et al. 2015)

1.9.2. Intracellular iron trafficking and utilization

Iron taken up by cells enters a cytosolic pool termed the ‘‘labile iron pool’’. The labile iron pool is destined to storage, export, or metabolic utilization. However, most of the labile iron pool is routed to mitochondria, where it is incorporated into heme and Fe-S clusters. Of note, iron acquired from Tf-Fe2 endocytosis may be transferred from endosomes to mitochondria by ‘‘kiss-and-run’’ via direct inter-organellar contacts, although the relative quantitative contribution of this pathway to mitochondrial iron acquisition remains to be clarified. (Hamdi et al. 2016)

1.9.3. Iron export

Cells export elemental iron in its ferrous state via Ferroportin. Mammalian ferroportin is particularly abundant in cells that maintain plasma iron levels as duodenal enterocytes, macrophages, and hepatocytes. (Drakesmith, Nemeth, and Ganz 2015) While ferroportin transports ferrous iron, efficient iron export requires its extracellular oxidation. Three multi-copper iron oxidases with distinct expression patterns are known: ceruloplasmin, hephaestin, and zyklopen. (Chen et al. 2010)

1.9.4. Iron storage

After entering the labile iron pool, iron can be stored within a cytosolic heteropolymer made of 24 subunits of heavy (FTH1) and light (FTL) ferritin

chains. Ferritin is a ubiquitous protein but the expression ratios of the two chains vary between tissues and in response to physiological conditions. FTH1 displays ferroxidase activity required for iron mineralization into the ferritin nanocage, while FTL promotes the transfer of electrons across the protein shell of the polymer. (Carmona et al. 2014) Iron sequestered in ferritin constitutes a store that can be mobilized by ferritin degradation. In iron-deficient cells, NCOA4 (Nuclear Receptor Coactivator 4) interacts with FTH1 and targets the ferritin complex for autolysosomes mediated degradation, a process called "ferritinophagy"; ferritinophagy is conversely suppressed in iron-loaded cells due to increased NCOA4 turnover. (Dowdle et al. 2014)

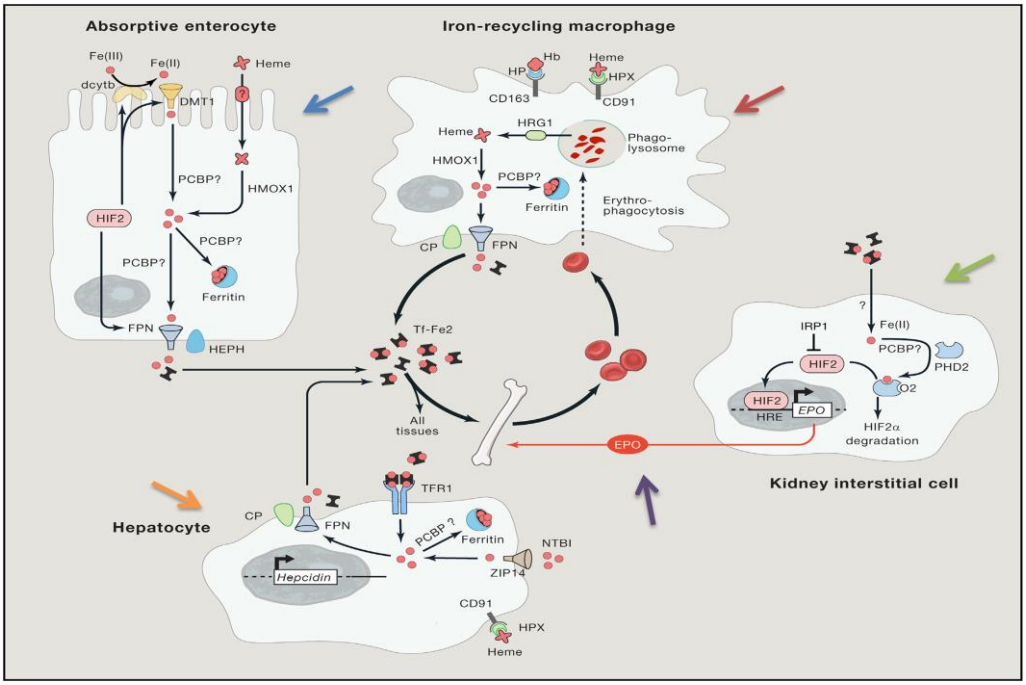

Figure 1.7: Systemic Iron Homeostasis. Enterocytes **(blue arrow)** take up elemental iron from the intestinal lumen via DMT1. At the basolateral side iron is oxidized to be released to the bloodstream via FPN and to be loaded onto Tf.. Tf-Fe2 is delivered to tissues via the bloodstream and is mostly used for the hemoglobinization of new red RBCs. Specialized tissue macrophages **(red arrow)** degrade senescent RBCs, releasing heme into the phagolysosome. If not used, iron is stored in hepatocytes. Peritubular fibroblasts of the kidney **(green arrow)** sense iron and oxygen deficiency and release EPO **(violet arrow)** to enhance erythropoiesis. Modified from Muckenthaler et al, 2017

1.9.5. Iron and liver

Liver is the main organ involved in iron metabolism as it orchestrates systemic iron balance by producing and secreting hepcidin. Hepcidin mainly acts inducing degradation of ferroportin and controls iron entry into the bloodstream from dietary sources, iron recycling macrophages, and body stores (Wang and Babitt 2019). In hepatocytes, hepcidin is finely regulated by the BMP/SMAD pathway. (Figure 1.9) Bone morphogenetic proteins (BMPs) act by binding to the complex of type I and type II serine/threonine kinase receptors, inducing phosphorylation of the receptor-activated SMAD 1, SMAD 5, SMAD 8 (R-SMADs). This class of SMADs complex with SMAD-4 and, translocating to the nucleus, guides expression of target genes involved in iron metabolism, as hepcidin itself. (Wang et al. 2017). SMADs modulate their own balance, by transcriptionally activating the inhibitory SMADs (I-SMADs), SMAD6 and SMAD7, with a negative feedback. (Kautz et al. 2008) Beyond the BMPs binding to receptor, modulation of the pathway requires a complex machinery of membrane proteins that acts as co-receptor or that regulates the intracellular pathway in response to iron levels. Among them, the protein hemojuvelin (HJV) acts as BMP coreceptor and up-regulates hepcidin through BMP-SMAD pathway. (Babitt et al. 2006) Indeed, mutations in this gene are causative of juvenile hemochromatosis due to suppression in hepcidin production. (Papanikolaou et al. 2004) HJV exists also in a soluble form (sHJV), originated after cleavage by TMPRSS6 protein. Soluble HJV has the opposite function of decoy molecule, blocking pathway activation. (Silvestri et al. 2008) In addition to HJV, other two proteins implicated in pathogenesis of hemochromatosis were found to be crucial in regulation of BMP/SMAD pathway: HFE and TFR2. Protein-protein interactions between HFE, TFR1, and TFR2 link iron sensing to pathway regulation. Indeed, high concentrations of iron-bound transferrin dissociate HFE from TFR1, which then binds to TFR2. (Core, Canali, and Babitt 2014) Although molecular mechanism of iron overload due to mutations in these two genes are almost unknown, functional

studies demonstrated that all these proteins form a membrane associated complex for hepcidin activation. (D'Alessio, Hentze, and Muckenthaler 2012) Regarding hepcidin down-regulation, the main inhibitor is the transmembrane serine protease 6 (TMPRSS6 or matriptase-2, MT2). Mutations in this gene are associated to the iron refractory iron deficiency anemia (IRIDA) due to high hepcidin levels. TMPRSS6 inhibits the BMP/SMAD pathway activation by cleaving membrane HJV. (Silvestri et al. 2008) TMPRSS6 expression was transcriptionally regulated by the inhibitor of DNA binding 1 (ID1) that, in turn, is regulated through BMP-RE present in its promoter region. (Finberg et al. 2010)

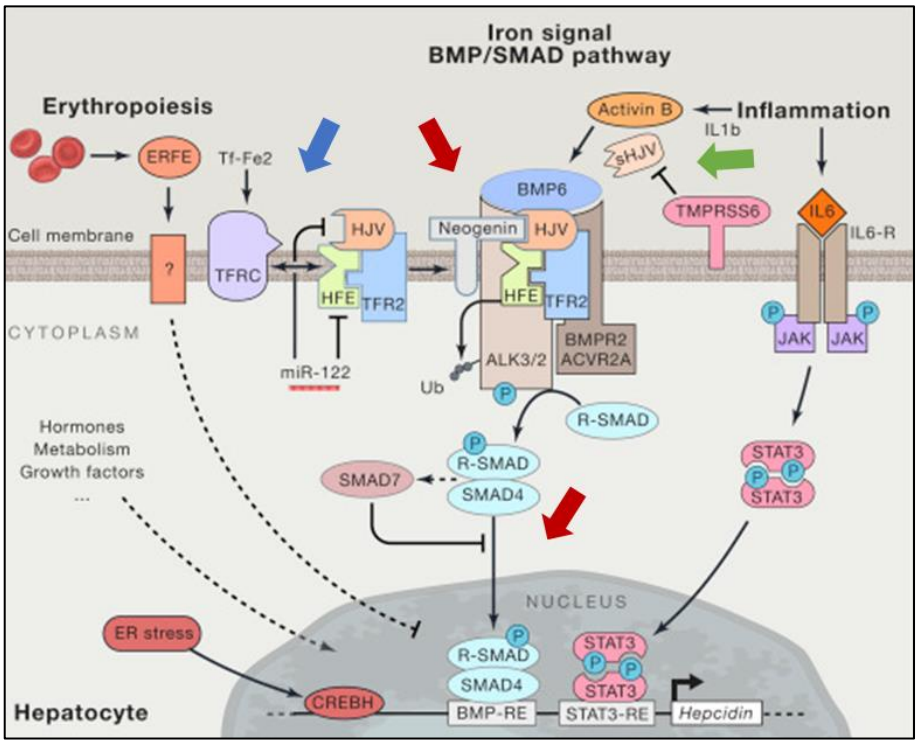

Figure 1.8: Regulation of hepcidin production in liver by BMP/SMAD pathway. High iron stores augment BMP6, which together with its co-receptor HJV activates type 1 and type 2 BMP serine threonine kinase receptors, leading to phosphorylation of receptor-activated SMADs (R-SMADs) proteins that complex with SMAD4, migrates to the nucleus and activates target genes **(red arrows)**. High concentrations of Tf-Fe2 displace HFE from TFR1, which then forms a complex with TFR2 and HJV to promote BMP/SMAD signaling to Hepcidin. **(blue arrow)** HFE additionally interacts with ALK3 and prevents its ubiquitination and degradation. BMP/SMAD signaling to hepcidin is suppressed by TMPRSS6, that generates a soluble form of HJV (sHJV). **(green arrow)** The pathway is also feedback inhibited by SMAD7. Modified from (Muckenthaler et al. 2017)

1.9.6. Iron and erythropoiesis

Most of the recycled iron (25 mg/day) is dedicated to hemoglobin synthesis. TFR1 mediates erythroid iron acquisition, so its expression is concordant to the maturation of erythroid progenitors. Mouse embryos lacking Tfr1 die because of severe anemia (and with neurologic abnormalities), whereas Tfr1 haploinsufficiency or dysfunction of other components of the TfR1 endocytotic cycle (such as DMT1, STEAP3) cause microcytic anemia because of defective iron utilization in mice. (Hentze et al. 2010) Under baseline conditions, iron flows mostly through the erythron and iron recycling macrophages. EPO controls the rate of erythropoiesis, which in turn inhibits hepcidin expression through ERFE to adjust iron efflux from macrophages and enterocytes. Hypoxia stimulates erythropoiesis through EPO to compensate for decreased oxygen transport. The resultant increase in ERFE production suppresses hepcidin and results in iron overload due to enhanced dietary iron absorption and iron release from macrophages. (Muckenthaler et al. 2017) (Figure 1.9) ERFE was discovered as an erythroid regulator that mediates hepcidin suppression during increased erythropoietic activity stimulated by endogenous or exogenous EPO and facilitates compensatory iron acquisition during the recovery from hemorrhage-induced anemia. (Kautz et al. 2014) In the bone marrow and the spleen, ERFE production is stimulated via STAT5. The canonical JAK2/STAT5 signaling pathway is known to mediate EPO response and stress erythropoiesis. (Porpiglia et al. 2012) Once activated, ERFE acts directly on the liver to decrease hepcidin production, so increasing iron availability for synthesis of new erythrocyte. In contrast to its adaptive role in the physiological recovery from anemia, ERFE can be pathologically involved in iron overload by suppressing hepcidin production as demonstrated in mice models of inherited anemias with ineffective erythropoiesis such as β-thalassemia (Kautz et al. 2015) and CDAII (Andolfo et al. 2019)

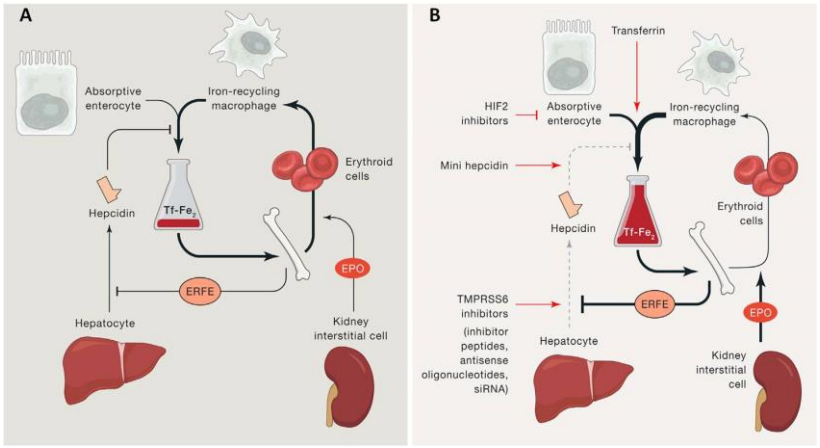

Figure 1.9. **Iron and erythropoiesis**. **A.** In physiological conditions, iron passes mostly through the erythron and iron recycling macrophages. Controls of erythropoiesis is mediated by EPO whose regulatory effects are mostly directed to inhibition of hepcidin through ERFE. **B**. In pathological conditions, as in case of ineffective erythropoiesis, regulation is mediated by the same actors. Firstly, the resulted hypoxia stimulates erythropoiesis through EPO to compensate the decreased oxygen transport. It results in hepcidin suppression, again through ERFE, and finally to an iron overload that derives from an increased dietary iron absorption and iron release from macrophages. Modified from Muckenthaler et al, 2017.

2. Aim of the study

This PhD project is focused on the study of molecular genetics and pathogenetic mechanism of iron overload in two inherited hemolytic anemias: DHS and CDAII. Both conditions are included in the group of hereditary hemolytic anemias characterized by severe hepatic iron overload. Our group identified disease causing genes of both the conditions: *PIEZO1* for DHS (Andolfo et al. 2013) and *SEC23B* for CDAII. (Schwarz et al. 2009)

The aims of this project are:

i) to find the molecular basis of hepatic iron overload in DHS with a particular focus on the possible direct involvement of PIEZO1 at hepatic level;

ii) to understand whether dyseritropoiesis have an exclusive role in determining hepatic iron overload in CDAII or a specific role of SEC23B could be assumed, beyond the erythroid involvement.

3. Materials and Methods

3.1 Patient collection and diagnostic workflow

DNA and plasma samples from patients were obtained after signed informed consent and according to the Declaration of Helsinki. Particularly, the clinical case described in this thesis project had referred to us from Hospital Galliera, Genova. The blood sample has been processed for hematological, rheology, and iron metabolism parameters. Genomic DNA preparation was performed as previously described. (Russo et al. 2013) To evaluate the quality of the extracted gDNA before the fragmentation, samples were quantified by NanoDrop 2000 (Thermo Scientific, Italy). Then, gDNA was loaded on 0.8% DNA agarose gel electrophoresis.

3.2 Libraries establishment and sequencing.

Genetic testing was achieved by targeted-NGS using an 86-gene custom panel for hereditary RBC defects. (Russo et al. 2018) For the probe design, coding regions, 5′UTR, 3′UTR, 50 bp flanking splice junctions were selected as regions of interest. The probe design was performed by the web-based tool SureDesign.(https://earray.chem.agilent.com/suredesign.htm,Agilent Technologies, USA). Sequence length was set at 150 x 2 nucleotides. The total probes' size was 298.393 kbp. Sample preparation was performed following the instruction's manufacturer for SureSelect^{QXT} Target Enrichment for the Illumina Platform - SureSelect Custom Tier1 1-499 kb (Agilent Technologies). High-throughput sequencing was performed by Illumina MiSeq. The alignment of the sequencing reads to genomic locations, the quality control metrics, and the identification of variants have been achieved by Alissa Align and Call software (v1.1.2-2, Agilent Technologies). Variant annotation and analysis have been performed by Alissa Interpret software (v5.2.6, Agilent Technologies). According to the guidelines of the American College of Medical Genetics and Genomics (ACMG), pathogenicity of each variant was evaluated considering population data, computational and predictive data,

functional data, and segregation data. Due to the large range of prevalence in the population of these heterogeneous disorders, we selected both rare and low-frequency variants (MAF < 0.01 and 0.05, respectively), as reported by gnomAD browser (https://gnomad.broadinstitute.org/).
InterVar (http://wintervar.wglab.org/) and Varsome (https://varsome.com/) web tools were used for the clinical interpretation. All the prioritized variants were confirmed by Sanger sequencing and by the analysis of inheritance pattern, whenever possible.

3.3 Hepcidin and ERFE dosage in plasma sample

Plasma levels of Hepcidin (Intrinsic HEPCIDIN IDx, Intrinsic Lifesciences) and ERFE (Intrinsic Erythroferrone IE; Intrinsic Lifesciences, CA, USA) were quantified using ELISA kits. Values of each sample were determined through the fitting of a four-parameter logistic curve, according to the manufacturer protocol. For ERFE assay, reference ranges were obtained by *in-house* healthy controls.

3.4 Cell cultures

The Huh7 and Hep3B cell lines were cultured in high-glucose Dulbecco's modified Eagle's medium (Sigma-Aldrich) and Essential modifies Eagle's medium (Sigma-Aldrich) supplemented with 10% (v/v) fetal bovine serum (Life Technologies; California, USA), 100 U/mL penicillin (Life Technologies), and 100 mg/mL streptomycin (Life Technologies), at 37°C in humidified air/CO_2 (19:1) atmosphere. The HepaRG human hepatocytes were cultured in complete basal medium (MH100-1, MH100-2; Lonza Ltd, Switzerland).
Huh7 cells were transfected with the pLVX-EF1α-IRES-ZsGreen1-*PIEZO1*-WT and pLVX-EF1α-IRES-ZsGreen1-*PIEZO1* mutant constructs (6 μg) for 48 h (FuGENE HD transfection reagent; Promega, Milan, Italy), and with the

pcDNA3.1-*PIEZO1*-WT and pcDNA3.1-*PIEZO1* mutant constructs (6 μg) for the Ca^{2+} assays (FuGENE HD transfection reagent).

After each transfection, mRNA and protein expression of PIEZO1 were evaluated. The presence of the mutations c.7367G>A, p.R2456H and c.7462G>A, p.R2488Q was also checked by PCR of the specific *PIEZO1* exon and by direct sequencing.

The lentiviral particles of sh-CTR, sh-70 and sh-74 (50 MOI) were generated as previously reported (Russo et al. 2016) and used to infect Huh7 cell line. After 48h of infection cells were maintained in puromicin (0.2 mg/mL) for 2 weeks and then analyzed for GFP positive expression. The sorted GFP positive cells were then assayed for *SEC23B* expression to verify the stability of the produced clones. Precision LentiORF Human SEC23A (3μg) (Horizon) was transfected into *SEC23B*-silenced Huh7 using FuGENE HD transfection Reagent (Promega). Cells were harvested at 0, 24 and 48 hours.

3.5 Limiting dilution and clonal expansion for single Hep3B – *PIEZO1*_R2456H KI clone selection.

Hep3B cells from the Synthego CRISPR-edited pool were diluted to 0.5 cells per 100 μl and plated on 96-wells to obtain the isolation and the expansion of single clones. Single clones were expanded and finally harvested. Genomic DNA extraction, PCR amplification of *PIEZO1* (ENST00000301015.14 – Exon 51), and Sanger sequencing were performed for each single colony from the CRISPR-edited pool to confirm the editing. Synthego's Inference of CRISPR edits (ICE) tool was used to analyze the sequence data. Synthego Performance Analysis, ICE Analysis. 2019. v2.0. Synthego (https://ice.synthego.com). ICE's output shows the relative contribution of each sequence presents in the cell clone (whenever mixed) highlighting WT and KI sequences and other indels. Moreover, statistical parameters are given as the total indels percentage, the model Fit (R2) that notifies how well the proposed indel distribution fits the sanger data of the

edited sample, and the KI-score that is the proportion of indels including the knock in insert.

3.6 Drugs treatment.

Huh7 overexpressing *PIEZO1* and Hep3B R2456H_KI cells were treated with 1.5µM of Yoda-1 (activator of PIEZO1, Cat. N° SML1558; Sigma-Aldrich) for 5 min without and with 5µM GsMTx-4 (inhibitor of PIEZO1; Cat. N° - ab141871 Abcam) for 30 min, as previously described, (Orvain et al. 2018) and then they were harvested for the subsequent analyses. Recombinant human BMP6 protein (507-BP-020; R&D Systems, Minneapolis, MN, USA) was used at 2 nM (90 minutes) for gene analyses and 6 nM (30 minutes) for protein ones. (Arezes et al. 2018) Tunicamycin (T7765, Sigma-Aldrich) was added at increasing concentration (0.5, 1.0, 1.5 µg/mL); (Lunde et al. 2017) DMSO was used as vehicle.

3.7 Calcium and potassium ion channel assay

Quantification of total intracellular Ca^{2+} was carried out in vitro using the Cal-520 assay (Cat. N° ab171868; AbCam). Cal-520 was diluted at 2.5 µM in cell culture medium, with 0.02% Pluronic F-127 (Cat. N° P2443; Sigma-Aldrich,). The plate was incubated for 90 min in a cell incubator, and then for 30 min at room temperature. Fluorescence was measured at excitation/emission wavelengths of 490/ 525 nm, and Ca2+ concentrations were calculated according to Equation (1):

$$[Ca2+]\ free = [F - Fmin]/[Fmax - F]/\ protein\ concentration \quad (1),$$

where F is the fluorescence of the indicator at the experimental Ca2+ levels, Fmin is the fluorescence in the absence of Cal-520, and Fmax is the fluorescence of the Ca2+-saturated probe.

Potassium ion channels and transporter activities were detected with the FluxOR™ Potassium Ion Channel Assay (Cat n. F10016-F10017, Life

technologies) Cells were incubated in the loading buffer at 24°C for 60 minutes, which was then replaced with the assay buffer and the stimulus buffer. All buffers were prepared according to the manufacturer's instructions. Fluorescence was measured every 2 seconds for 2 minutes using a kinetic dispense microplate reader, setting the excitation wavelength to 490 nm, and the emission wavelength to 520nm. Each sample was plated in quadruplicate. Data were presented as mean of the difference between fluorescence of each time point and fluorescence at 0 time. (ΔF)

3.8 RNA isolation, reverse transcription, and quantitative real-time PCR analysis

Total RNA was extracted from cells using Trizol reagent (Life Technologies). cDNA synthesis from total RNA (1 μg) was performed using SuperScript II First Strand kits (Life Technologies). Quantitative (q)RT-PCR was performed using the SYBR-green method, following standard protocols (ABI Prism 7900HT sequence detection system; Applied Biosystems). Real-time -PCR was performed using a standard TaqMan PCR kit protocol for *ID1* and *ID3* genes. Relative gene expression was calculated using the $2^{-\Delta Ct}$ method, where ΔCt indicates the differences in the mean Ct between the selected genes and the normalization control (β-actin). The qRT-PCR primers for each gene were designed using Primer Express software version 2.0 (Life Technologies).. The reactions were incubated in a 96-well plate at 95°C for 10 min, followed by 40 cycles of 95°C for 15 s, and 60°C for 1 min.

3.9 Protein isolation and western blotting analysis

Proteins were extracted from cells using RIPA lysis buffer in the presence of a protease inhibitor cocktail (Roche, Rotkreuz, Switzerland). Total protein extracts were analysed by SDS-PAGE, transferred to polyvinylidene difluoridemembranes (BioRad, Milan, Italy), and then incubated with the required combinations of the following antibodies: rabbit polyclonal anti-PIEZO1 (Cat. N° 15939-1-AP; 1:250 dilution; Proteintech, UK) rabbit polyclonal anti-pErk1/pErk2 (Cat. N° ab32538; 1:250 dilution; AbCam); rabbit polyclonal anti-Erk1/2 (Cat. N° ab17942; 1:1000 dilution; AbCam); rabbit anti-SEC23B (1:1000; SAB2102104; Sigma Aldrich); polyclonal rabbit anti-SEC23A (GTX109488 1:1000; GeneTex); Rabbit anti-Ferritin (1:1000; abcam, ab75973); polyclonal rabbit Anti-Transferrin Receptor 2 (1:1000, Abcam, ab80194); monoclonal rabbit anti-HFE (1:1000. Abcam, ab133639); monoclonal rabbit anti-TMPRSS6 (1:1000, Abcam, ab56180); monoclonal rabbit anti-pSMAD 1-5-8 (1:1000, Cell Signalling, 13820); polyclonal rabbit anti-tSMAD 1-5-8 (1:1000, abcam, ab13723); rabbit anti-GAPDH (1:1000; 2118, Cell Signaling Technology). The membranes were incubated with the enhanced chemiluminescence substrate (Supersignal West Pico chemiluminescent substrate kits; Thermo Fisher Scientific, Milan, Italy). The labeled band was visualized and densitometric analyses were performed using the Chemidoc and Quantity One software (BioRad).

3.10 Differential Proteomics analysis

KI and WT cells were parallelly expanded in quadruplicate for proteomics analyses and treated with Yoda-1 (1.5 μM) to chemically activates PIEZO1. After 30 minutes, cells were harvested and pelleted. Proteomics experiments and raw analyses were performed at TIGEM Proteomics facility (Pozzuoli, NA). To analyze the huge amount of data resulting from proteomics (4265 total proteins identified), we firstly filtered raw data for all proteins that significantly differed in PIEZO_KI compared to PIEZO1_WT (**225**, 5.3%). Then, we

divided the upregulated (**147**) from the downregulated ones (**78**), and finally a KEGG pathway analysis was performed by using DAVID Bioinformatics Resources 6.8. (Huang da, Sherman, and Lempicki 2009).

3.11 Statistical and bioinformatics analysis.

Quantitative data were compared using the Mann-Whitney test for expression analysis in patients and controls and Student's t test for all the other analysis. A two-sided $p<0.05$ was considered statistically significant.

4. Results

4.1 Analysis of iron balance and ineffective erythropoiesis markers in patients with DHS1 and CDAII.

We first analyzed the levels of hepcidin in the plasma of 54 patients with CDAII and 42 DHS1 patients enrolled in our International Registry of Hereditary Anemias. Both cohorts of patients showed lower hepcidin levels compared to the median value of reference ranges. (Figure 4.1 A) We also evaluated the plasma concentrations of the negative erythroid regulator of hepcidin, ERFE, and we observed slightly increased levels compared to reference ranges (obtained by measuring *in house* controls) in DHS1 patients. Besides, CDAII patients exhibited tendentially increased levels of ERFE, although in some cases, levels appear comparable to those of healthy controls (Figure 4.1 B). For this reason, we stratified CDAII patients according to the degree of anemia expressed in terms of Hb concentration. Particularly, we found that patients with lower Hb concentration (<10.5 g/dL) expressed higher ERFE levels than mildly affected patients (Hb > 10.5 g/dL) but not significantly. (Figure 4.1 C) Indeed, we associated hepcidin levels to ERFE concentration in the entire subset of CDAII patients observing that the correlation was not always relevant. (Figure 4.1 D)

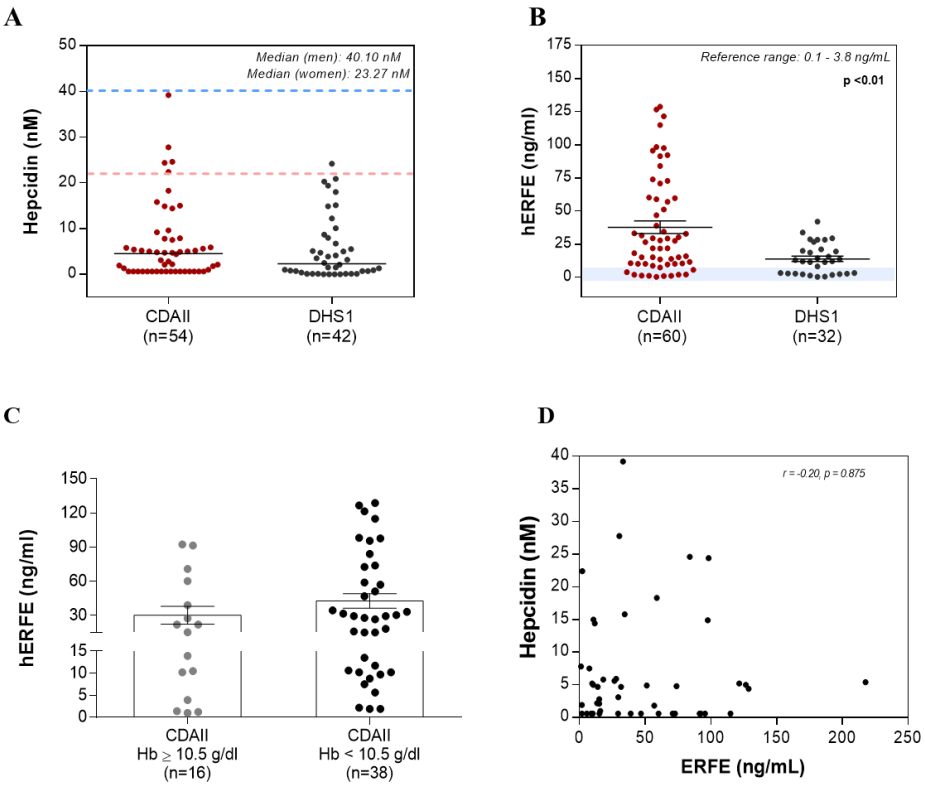

Figure 4.1: Hepcidin, ERFE and EPO expression in plasma from patients with DHS1 and CDA II. A. Quantification of hepcidin levels in plasma from 54 patients with CDA II and 42 patients with DHS1 by ELISA assay. Reference median values are indicated (dashed blue and pink lines, respectively for men and women). **B.** Quantification of ERFE protein levels in plasma from 60 patients with CDA II and 32 patients with DHS. Reference ranges obtained from "*in house"* controls were indicated and showed as light blue shadow. pValue as indicated (Mann Whitney-tests < 0.01 CDAII *vs* HC, DHS1 *vs* HC, CDAII *vs* DHS1). **C.** Box plot showing ERFE levels in plasma sample of CDAII patients stratified according to Hb levels. **D.** Scatter plot showing correlation between Hepcidin levels (nM) and hERFE concentration (ng/mL) in CDAII patients. Data are means ± SEM of two replicates.

4.2 Physiological role of PIEZO1 in the liver

Due to the only slight increase of ERFE in DHS1 patients we hypothesized a direct role of PIEZO1 at hepatic level. We firstly measured its expression levels in liver. By searching in the R2 webtool database (Genomics Analysis and Visualisation Platform), we found high expression of *PIEZO1* across several tissues, including liver (Figure 4.2 A). Then, we analyzed PIEZO1 mRNA and protein expression in three hepatic cell lines confirming that it was highly expressed (Figure 4.2 B, C). On this basis, we analyzed the physiological role of PIEZO1 in the liver by determining the intracellular Ca^{2+} concentrations in two different cell systems: Huh7 cells, as a human hepatoma cell line, and HepaRG cells, as human primary hepatocytes. We used the chemical activator of the PIEZO1 channel, Yoda-1 (as PIEZO1 is a mechanoreceptor not active without stimulation) and GsMTx-4 as inhibitor. After PIEZO1 activation by Yoda-1, the intracellular Ca^{2+} concentrations were significantly higher compared to the untreated Huh7 and HepaRG cells (Figure 4.2 D). On the contrary, the addition of GsMtx-4 reduced intracellular Ca^{2+} concentrations (Figure 4.2 D). The iron status was assessed by measuring gene expression of *HAMP*, encoding for hepcidin, in the two cell lines under activating and inhibiting conditions. *HAMP* expression was significantly reduced by Yoda-1 treatment in both Huh7 and HepaRG cells, while addition of GsMTx-4 restored *HAMP* expression. (Figure 4.2 E, F).

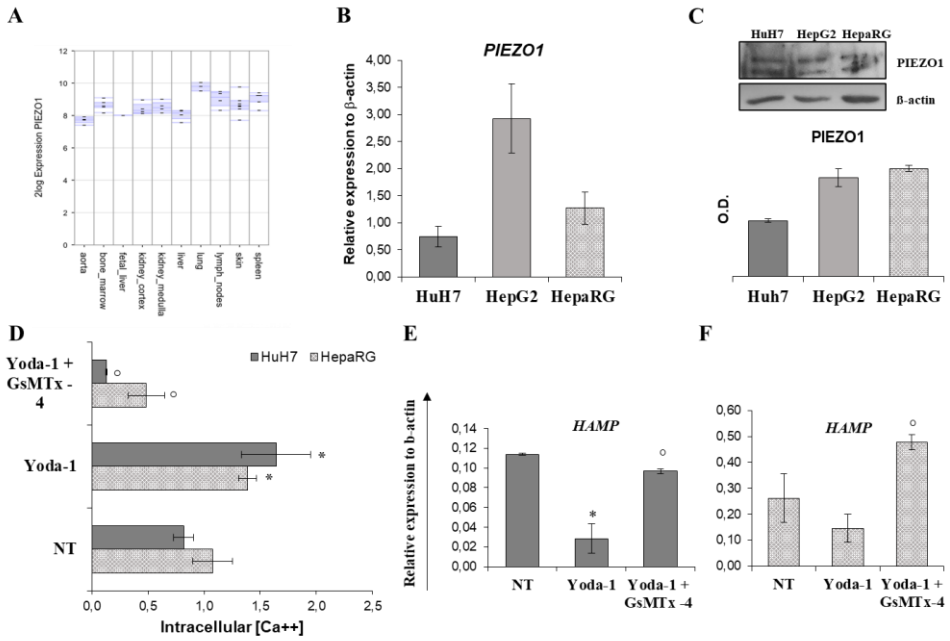

Figure 4.2: **Physiological role of PIEZO1 in the liver. A.** *In-silico* expression analysis of *PIEZO1* using the R2 webtool. BoxDotPlots obtained using MegaSampler analysis show *PIEZO1* expression in normal tissues from different datasets. Data are 2log transformed. **B**. Quantification of *PIEZO1* mRNA levels normalized to β-actin in different hepatic cell lines at steady-state. Data are means ± standard deviation of three independent experiments. **C.** Representative immunoblot of PIEZO1 protein expression in different hepatic cell lines at steady state. **D.** Quantification of total intracellular Ca^{2+} concentrations in HepaRG and Huh7 cells not treated (NT), treated with the PIEZO1 activator, Yoda-1 (6 µM), and with Yoda-1 (6 µM) plus the PIEZO1 inhibitor GsMTx-4 (5 µM). Data are means ± standard deviation of three experiments and are normalized for protein concentrations (*$p < 0.05$, NT vs. Yoda-1; $p < 0.05$, Yoda-1 vs. Yoda-1 plus GsMTx-4). **E and F.** Quantification of *HAMP* mRNA levels normalized to β-actin in the HepaRG and Huh7 cells not treated (NT), treated with the PIEZO1 activator, Yoda-1, and with Yoda-1 plus GsMTx-4. Data are means ± standard deviation of three experiments (*$p < 0.05$, NT vs. Yoda-1; °$p < 0.05$, Yoda-1 vs. Yoda-1 plus GsMTx-4).

4.3 Establishment of hepatic cell line over-expressing PIEZO1 WT and mutants and evaluation of iron and calcium status.

To study the pathogenic mechanism of DHS1 iron overload in the hepatic compartment, we carried out further functional analysis using the Huh7 cells. *PIEZO1*-WT, two *PIEZO1* gain-of-function mutants, R2456H and R2488Q, were expressed for 48 h in this cell line.

The over-expression was tested at both protein and mRNA levels (Figure 4.3 A) and Sanger sequencing confirmed the presence of both the point mutations. (c.7367G>A, p.R2456H and c.7462G>A, p.R2488Q) (Figure 4.3 B) Here, we examined expression of *HAMP* gene that was significantly down-regulated in cells expressing the two *PIEZO1* mutants compared to WT. (Figure 4.3 C). As *PIEZO1* gain-of-function mutations have been associated with increased intracellular Ca^{2+} content in RBCs, (Andolfo et al. 2015; Glogowska et al. 2017; Gudipaty et al. 2017) we measured intracellular calcium concentration in cells expressing both *PIEZO1* mutants. We found a significantly increase in calcium content after treatment with Yoda-1. The increased intracellular Ca^{2+} concentration was largely lost after the addition of GsMTx-4. (Figure 4.3 D).

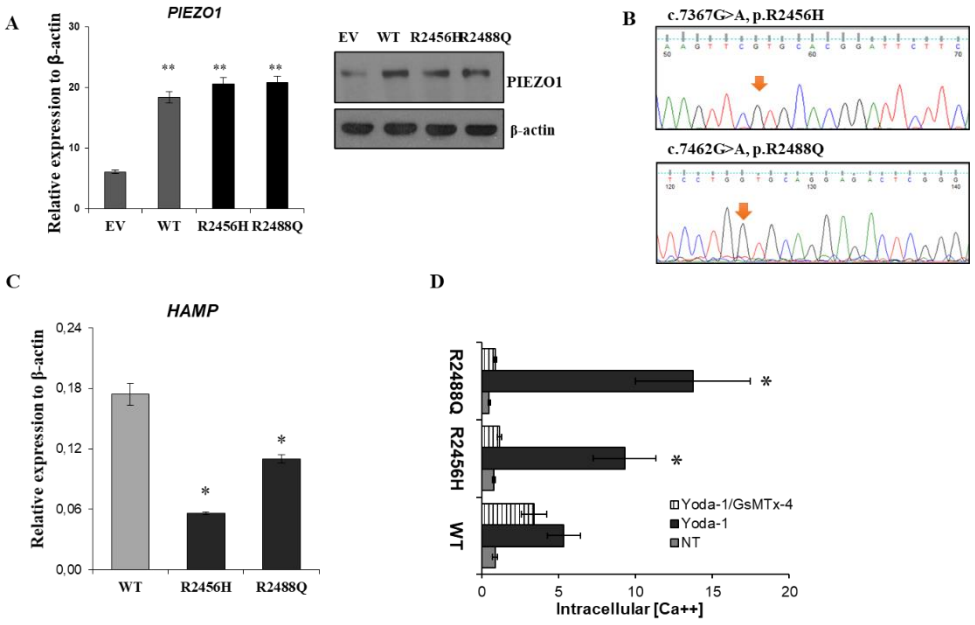

Figure 4.3: A. Quantification of *PIEZO1* mRNA (left panel) and representative immunoblots of PIEZO1 protein (right panel) in Huh7 cells expressing the empty vector (EV), *PIEZO1*-WT and the R2456H and R2488Q mutants. β-actin is the loading control. Quantified data are means ± standard deviation of three experiments with similar results (**p<0.01 *vs* EV). **B.** Representative electropherograms of exon 51 of *PIEZO1* showing the mutations c.7367G>A, p.R2456H and c.7462G>A, p.R2488Q in the hepatic mutant cells. **C** Quantification of *HAMP* mRNA levels normalized to *β-actin* in Huh7 cells expressing human *PIEZO1*-WT, *PIEZO1*-R2456H and PIEZO1-R2488Q. Data are means ± standard deviation of three independent experiments (*p < 0.05, *vs.* relevant WT). **D.** Quantification of total intracellular Ca^{2+} concentrations in Huh7 cells expressing *PIEZO1*-WT and the mutants, as non-treated (NT) and treated with the PIEZO1 activator Yoda-1 (1.5 µM), and with the PIEZO1 inhibitor, GsMTx-4 (5 µM) plus Yoda-1 (1.5 µM). Data are means ± standard deviation of three experiments, normalized to the protein concentrations (*p < 0.05, *vs.* relevant WT-Yoda-1)

4.4 Cell signaling analysis: MAPK and BMP/SMADs pathways in PIEZO1 mutants

We hypothesized that the link between the mutations of *PIEZO1* and the iron overload seen in DHS1 patients might relate to PIEZO1-Ca^{2+}-triggered ERK1/2 signaling (Cahalan et al. 2015; Liang et al. 2017; Luo 2017; Piddini 2017) and in turn the modulation of the BMP/SMADs pathway.(Sugimoto et al. 2017; Utsugisawa et al. 2006)

To examine the link between the intracellular Ca^{2+} concentrations and *HAMP* gene expression, Huh7 cells were treated with the Ca^{2+} ionophore A23187 (4 μM), to mimic the Ca^{2+} overload. In parallel with the increased intracellular Ca^{2+} concentrations upon the A23187 treatment, the *HAMP* gene expression was down-regulated in ionophore-treated cells, compared to the control. (Figure 4.4 A)

Then, we analyzed ERK1/2 phosphorylation in Huh7 cells, and we observed that gain-of-function mutants showed a more pronounced phosphorylation of ERK1/2 compared to WT (Figure 4.4 B, C) according to the higher intracellular Ca^{2+} concentrations seen. Besides, SMAD1/5/8 phosphorylation was lower in mutants compared to WT. (Figure 4.4 B, C) To confirm the direct implication of these *PIEZO1* mutations in the unbalanced ERK and BMP-SMADs pathways, phenotype rescue was carried out with PIEZO1 inhibitor, to determine whether GsMTx-4 treatment can modulate the phosphorylation of both ERK1/2 and of SMAD1/5/8. Indeed, addition of GsMTx-4 blocked ERK1/2 phosphorylation. Besides the SMAD1/5/8 phosphorylation levels were restored to WT levels in both the mutants when treated with GsMTx-4. (Figure 4.4 B, C, right panels).

To further investigate the interplay between ERK1/2 and SMAD1/5/8, Huh7 cells were treated with PD0325901, a potent MEK1 and MEK2 inhibitor that is highly selective for inhibition of ERK1/2 phosphorylation. Of note, this resulted in reduced phosphorylation of ERK1/2 in the Huh7 cells (Figure 4.4 D), with the consequent increased phosphorylation of SMAD1/5/8 due to the

inhibition of ERK1/2. (Figure 4.4 D). The altered BMP/SMADs signaling was also investigated by analyzing the mRNA levels of several target genes: *SMAD6*, *SMAD7*, *ID1*, and *ID3*. All genes resulted significantly down-regulated in *PIEZO1* gain-of-function mutants compared to WT (Figure 4.5 A). Finally, gene and protein expression of TMPRSS6 was also examined, as TMPRSS6 is indirectly regulated by the SMADs cascade.(Meynard et al. 2011) Both protein and mRNA levels of TMPRSS6 resulted significantly lower in mutants compared to WT. (Figure 4.5 B).

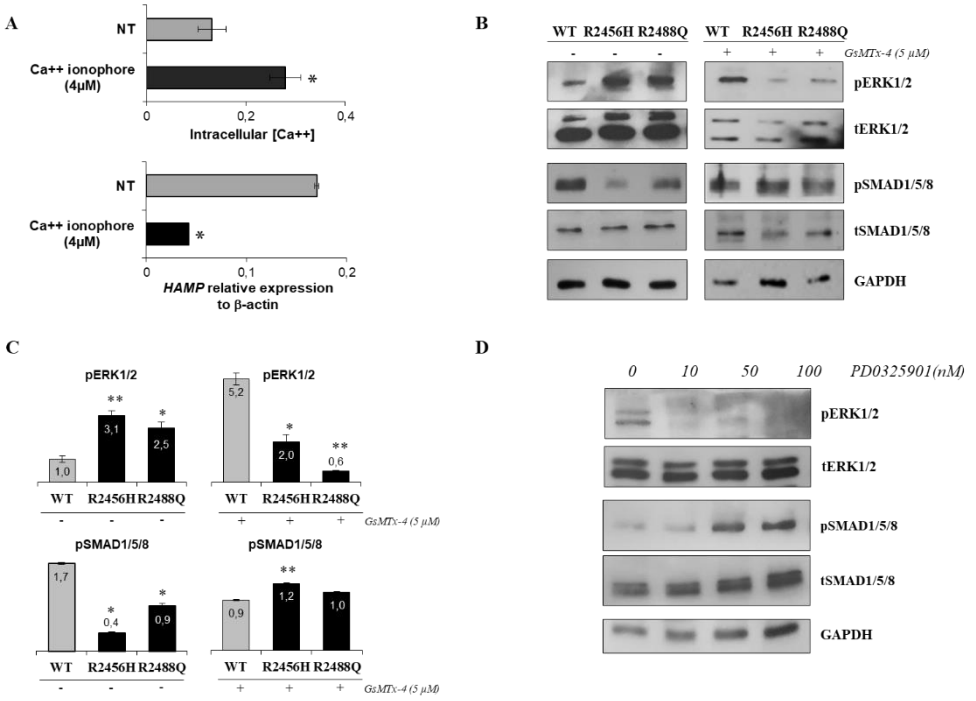

Figure 4.4: Pathway analysis and calcium overload: A. Upper panel: quantification of intracellular Ca^{2+} concentrations using the Cal520 assay in Huh7 cells without (NT) and with calcium ionophore A23187 addition**; lower panel**: *HAMP* mRNA levels normalized to *β-actin* in Huh7 cells untreated and treated with calcium ionophore A23187. **B.** Representative immunoblots of pERK1/2, tERK1/2, pSMAD1/5/8 and tSMAD1/5/8 proteins in total cells lysate of Huh7 cells expressing *PIEZO1*-WT and mutants not treated and treated with GsMTX-4. GAPDH is the loading control. **C.** Quantification by densitometric analysis from Huh7 cells of three separate Western blots with similar results. **D**. Representative immunoblots is showing pERK1/2 and tERK1/2 and pSMAD1/5/8 and tSMAD1/5/8 protein expression in Huh7 cells treated with PD0325901 (as indicated). GAPDH is the loading control. Data are means ± standard deviation (*$p < 0.05$, vs. relevant WT; ** $p < 0.001$ vs. relevant WT).

4.5 Rescue of the imbalanced iron metabolism by GsMTx-4

To further confirm the direct effects of *PIEZO1* gain-of-function mutants on BMP/SMAD signaling, *HAMP* and *ID1* gene expression were determined following GsMTx-4 treatment. We observed that expression of both genes in both mutants were restored after treatment with GsMTx-4 compared to WT in Huh7 cells (Figure 4.5 C).

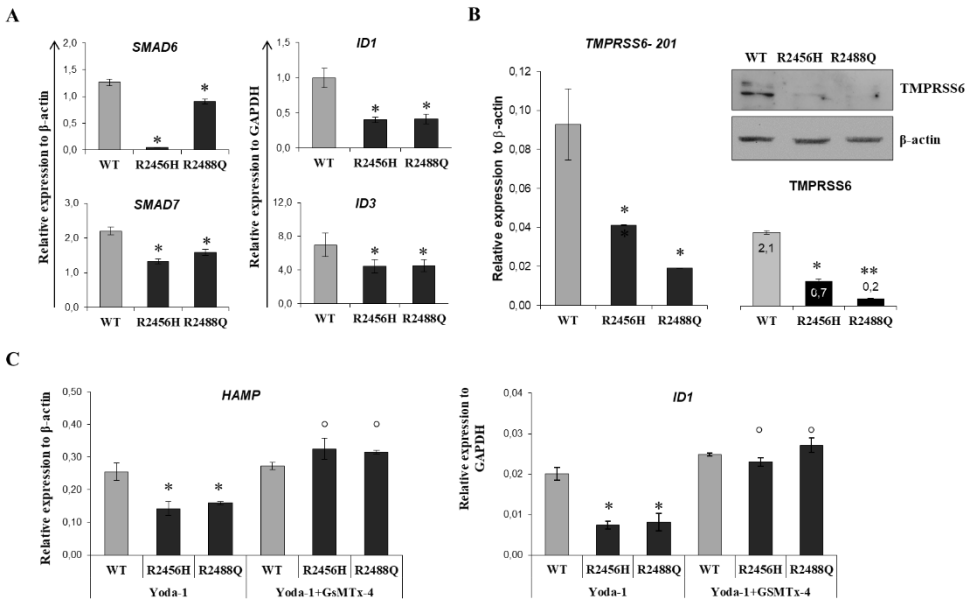

Figure 4.5: Evaluation of BMP/SMAD targets in hepatic system expressing *PIEZO1*-WT and mutants, and phenotype rescue.
A. Quantification of *SMAD6, SMAD7* (normalized to *β-actin), ID1* and *ID3* (normalized to *GAPDH*, TaqMan assay) mRNA levels in Huh7 cells expressing *PIEZO1*-WT and mutants. **B. Left panels**: quantification of *TMPRSS6-201* transcript (ENST00000346753.8, CCDS13941, NM_153609) levels (normalized to *β-actin*) in Huh7 cells expressing *PIEZO1*-WT and mutants. **Right panels**: representative immunoblots of TMPRSS6 protein levels in Huh7 cells expressing *PIEZO1*-WT and mutants. Quantification by densitometric analysis of three separate Western blots with similar results. Data are means ± standard deviation of three independent experiments (*p < 0.05, ** p< 0.01 vs. relevant WT) **C.** Quantification of *HAMP* (left) and *ID1* (right) mRNA levels normalized to *β-actin* and *GAPDH*, respectively, in Huh7 cells expressing *PIEZO1*-WT and mutants and treated with PIEZO1 activator Yoda-1 and without or with the PIEZO1 inhibitor GsMTx-4 (as indicated). Data are means ± standard deviation of three independent experiments (*p < 0.01, *vs.* relevant WT; ° p < 0.05, *vs.* relevant Yoda-1 treated cells).

4.6 Creation and characterization of Hep3B engineered cell line for *PIEZO1* R2456H variant.

The lack of a reliable model for the study of DHS, led us to create a cellular hepatic model that presents the R2456H variant, by the means of CRISPR-CAS9 technology. In order to choose the best cellular model, different cell lines (Huh7, HepG2 and Hep3B) were tested by CGH array analysis. Among them, we selected Hep3B cells that were the only ones presenting the correct copy number of *PIEZO1* gene. The insertion of the R2456H variant in Hep3B cells was performed in service by Synthego (Menlo Park, California). The KI pool, containing only 18% of modified cells, (Figure 4.6 A) was diluted and amplified until obtaining single clones. These clones were sequenced by Sanger Sequencing on exon 51 of *PIEZO1* and analyzed by The Synthego ICE Analysis tool (see M&M, section 3.5). The chosen clone presented the variant in heterozygous state (KI score 50%) and a R^2 of 0.97. An insertion of one nucleotide was reported in 46% of cell population but with no functional effect as demonstrated by gene and protein expression analysis. (Figure 4.6 B). This clone, named PIEZO1_KI, was tested for *PIEZO1* gene and protein expression that, as expected, resulted unvaried. (Figure 4.6 C) Besides, we quantified the potassium channel activity that in PIEZO1_KI resulted strongly increased compared to PIEZO1_WT confirming the gain of function of the selected variant. (Figure 4.6 D) We confirmed most of the previous data on the new model. Firstly, we tested for intracellular calcium content on both untreated cells (NT), Yoda1-activated cells (Yoda-1) and cells rescued with PIEZO1 inhibitor (GsMTx-4) confirming that the activation increased calcium concentration while the inhibition of the channel restored calcium concentration inside the cells. (Figure 4.7 A) The unbalanced iron status was assessed by evaluating *HAMP* gene expression that resulted strongly and significantly reduced in PIEZO1_KI compared to WT. (Figure 4.7 B) According to *HAMP* reduction, we observed a downregulation of the BMP/SMAD pathway. Particularly, at

mRNA level, *ID1* and *SMAD6* resulted reduced in PIEZO1_KI compared to WT_PIEZO1 as phosphorylation of SMAD 1/5/8 that follows the same tendency. (Figure 4.7 C, D)

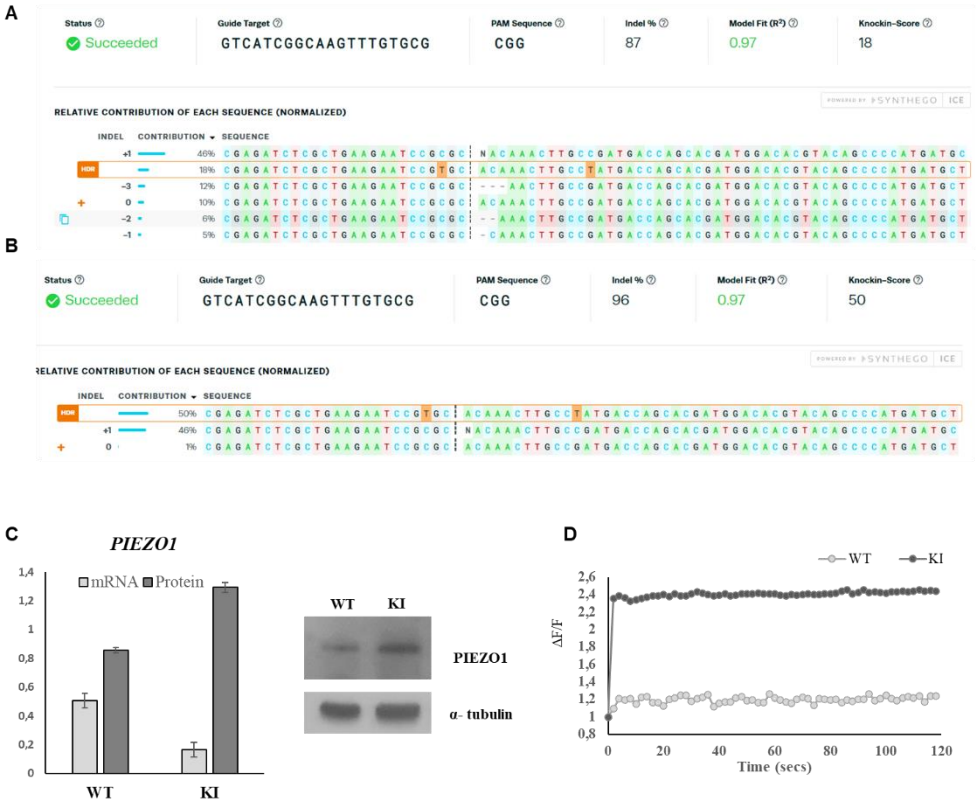

Figure 4.6: Establishment and characterization of R2456H KI-Hep3B cells. Inferred sequences of the mixed edited population **(A)** and in single selected clone **(B)** and their relative proportions. Cut sites are represented by black vertical dotted lines; the wild-type sequence is marked by a "+" symbol on the far left; the knocked in sequence is marked with orange rectangle**.** gRNA sequence, PAM, indel percentage, R^2 and knock-in score are shown at the top of the alignment. Contributions were obtained by ICE tool. **C. (left panel)** Histograms showing mRNA (light grey) and protein (dark grey) expression of PIEZO1 in PIEZO1_WT and PIEZO1_KI cells. Quantification was performed by densitometric analysis of three separate Western blots with similar results. **(Right panel)** Representative immunoblot of PIEZO1 in Hep3B_WT and PIEZO1_KI cells. Data are means ± standard deviation of three independent experiments and are normalized on α-tubulin. **D.** Quantification of potassium channel activity in PIEZO1_WT and PIEZO1_KI treated with Yoda-1. ΔF/F is the difference between the mean of fluorescence (four replicates) at each time (2'' for 2') and fluorescence at 0 time.

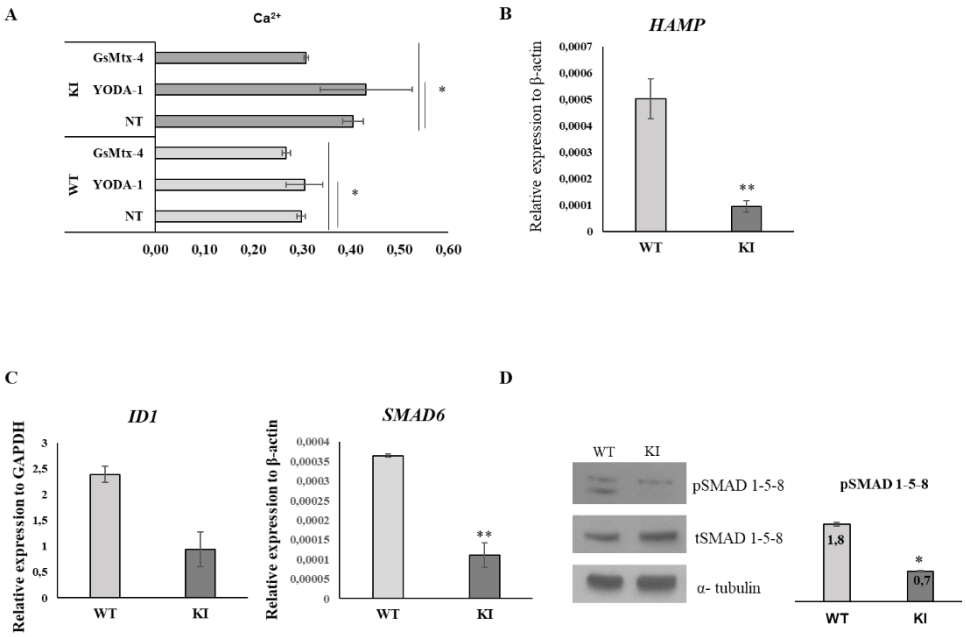

Figure 4.7 A. Quantification of total intracellular Ca^{2+} concentrations in PIEZO1_WT and PIEZO1_KI non-treated (NT) and treated with the PIEZO1 activator Yoda-1 (1.5 µM), and with the PIEZO1 inhibitor, GsMTx-4 (5 µM) plus Yoda-1 (1.5 µM).. **B.** Quantification of *HAMP* mRNA levels normalized to *β-actin* in PIEZO1_WT and PIEZO1_KI. **C.** Quantification of *ID1 and SMAD6* mRNA in PIEZO1_WT and PIEZO1_KI in PIEZO1_WT and PIEZO1_KI. **D. (left panel)** Representative immunoblots of pSMAD1/5/8 and tSMAD1/5/8 proteins in total cells lysate of PIEZO1_WT and PIEZO1_KI cells. A- tubulin is the loading control**.** Quantification by densitometric analysis of three separate Western blots with similar results is shown in **right panel**. Data are means ± standard deviation (*$p < 0.05$, vs. relevant WT; ** $p < 0.001$ vs. relevant WT).

4.7 Differential proteomic analyses of PIEZO1_WT and PIEZO1_KI R2456H

To widen our knowledge of the effects of *PIEZO1* GoF mutation at hepatic level, we performed a differential proteomic analysis on PIEZO1_KI and PIEZO1_WT Hep3B cells. Raw data obtained by proteomic analysis were filtered as described in section 3.10 of M&M. Results of KEGG pathway analyses were summarized in Figure 4.8A. As pathway of interest, we selected "regulation of actin cytoskeleton" including some significantly up-regulated proteins. All the proteins took in count for pathway classification were

individually analyzed. (Figure 4.8B) Regarding the regulation of actin cytoskeleton pathway, in addition to R-Ras and MAP2K1 that belong to the MAPK pathway, the other proteins that mainly act in cytoskeleton organization are also reported to indirectly regulate the same pathway. To date, all these proteins were up regulated in PIEZO1_KI cells compared to PIEZ01_WT.

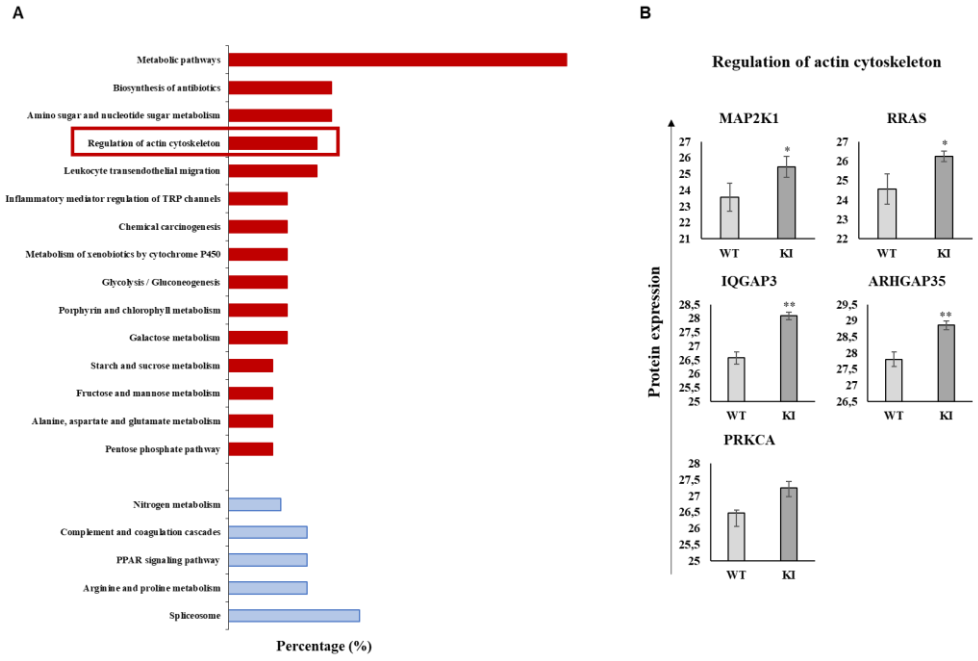

Figure 4.8 KEGG pathway analysis and single protein quantifications. **A.** KEGG pathway enrichment analysis of differentially expressed proteins between PIEZO1_WT and PIEZO1_KI Hep3B cells. Upregulated (red) and downregulated (blue) pathways are shown. **B.** Histograms showing quantification of single proteins composing the *regulation of actin cytoskeleton* pathway. Data are means ± standard deviation of three separate quantifications. (*$p < 0.05$, vs. ** $p < 0.001$ vs. relevant WT).

4.8 Establishment of hepatic model stably silenced for *SEC23B* and assessment of iron status.

To reproduce *SEC23B* loss-of-function mutations at hepatic level, Huh7 cell line silenced for *SEC23B* were generated by the means of small hairpin (sh) RNA method. The silencing efficiency was tested trough qRT-PCR and Western blot analyses of SEC23B (Figure 4.9 A) and, on selected clones, of its paralogue SEC23A. (Figure 4.9 B). We found that *SEC23B* expression was down-regulated in both sh74-*SEC23B* and sh70-*SEC23B* clones compared to sh-CTR cells. Moreover, as sh70-*SEC23B* cells showed down-regulation of *SEC23A* gene and protein expression, we excluded the clone from further analysis. The selected sh74-*SEC23B* clone was tested for *HAMP* and *Ferritin* expression to determine the iron status. We found that *HAMP* expression was reduced compared to sh-CTR cells (Figure 4.9 C) while *Ferritin* levels were increased in silenced clone at both mRNA and protein levels (Figure 4.9D).

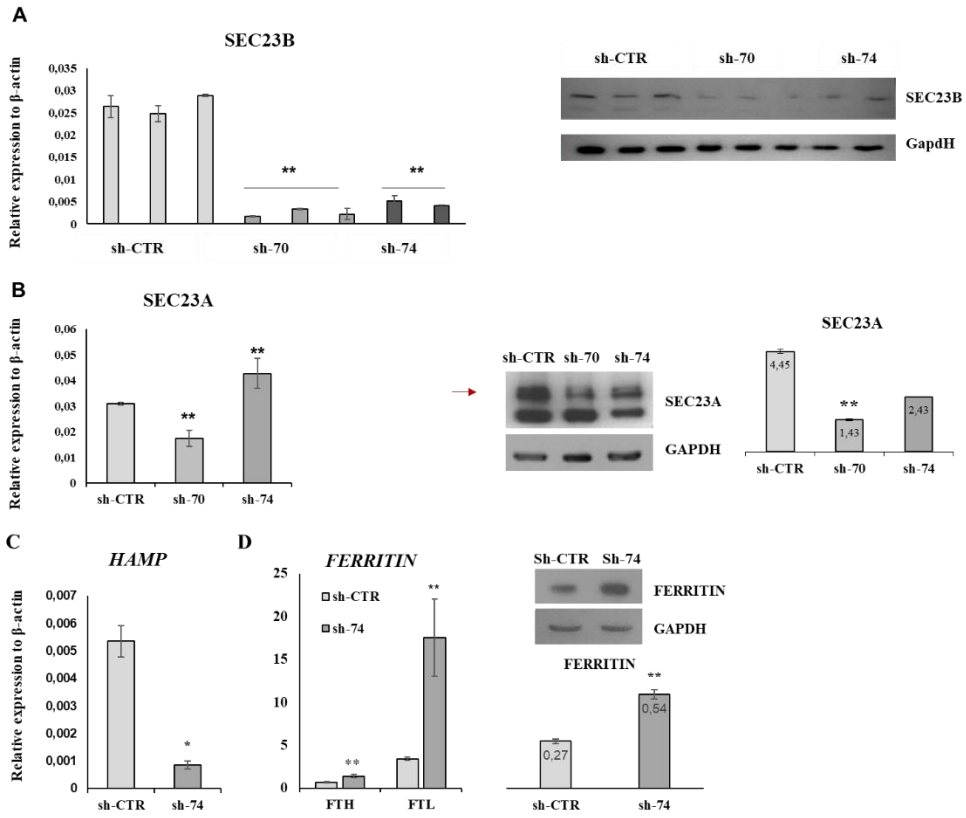

Figure 4.9. Establishment of SEC23B stably silenced clones and determination of iron status. A. (left panel) Quantification of *SEC23B* mRNA levels normalized to β-actin in Huh7 cell line silenced for *SEC23B*. Data are means ± standard deviation of three independent experiments. (**p < 0.01, sh-CTR vs sh-70 and shCTR vs sh-74). **(right panel)** Representative immunoblot of SEC23B and GAPDH in Huh7 control and SEC23B- silenced cells. **B.** Quantification of *SEC23A* mRNA levels normalized to β-actin **(left panel)** and representative immunoblot **(middle panel)** in sh-CTR, sh-70 and sh-74 Huh7. **Right panel**. Quantification by densitometric analysis of three separate Western blots with similar results. Data are means ± standard deviation of three independent experiments. (**p < 0.01, sh-CTR vs sh-70) **C.** Quantification of *HAMP* mRNA levels normalized to β-actin. Data are means ± standard deviation of three independent experiments. (*p < 0.05, sh-CTR vs sh-74 C. **D.** Quantification of light and heavy chain of *Ferritin* normalized to β-actin in the Huh7 sh-CTR and Huh7 sh74-*SEC23B*. (**p < 0.01, shCTR vs sh74) **(Right panel).** Representative immunoblot of Ferritin protein expression in sh74-*SEC23B* and shCTR Huh7 **(upper)**. Quantification by densitometric analysis of three separate Western blots with similar results. Data are means ± standard deviation of three independent experiments **(lower)**. (**p < 0.01, sh-CTR vs sh-74)

4.9 BMP/SMADs pathway alteration in *SEC23B* loss of function hepatic cells

To further characterize the alteration of iron status in *SEC23B*-silenced Huh7 cells, we evaluated protein levels of pSMAD 1/5/8 and its inhibitor SMAD7. We found that phosphorylation was strongly reduced in sh74-*SEC23B* compared to sh-CTR cells while SMAD7 protein level were increased compared to control (Figure 4.10 A). The inhibition of BMP6/SMADs pathway was also assessed by mRNA analysis of target genes. Particularly, we tested *SMAD6*, *ID1* and *ID3* genes expression that resulted down-regulated in sh74-*SEC23B* compared to sh-CTR. (Figure 4.10 B).

Finally, we tested whether the loss of *SEC23B* affected the BMP/SMADs pathway activation. To this aim, we treated sh-CTR and sh74-*SEC23B* cells with recombinant BMP6 and we evaluated the *HAMP* gene expression and SMAD 1-5-8 phosphorylation. In both cases we found that sh74-*SEC23B* cells were more resistant to pathway activation after BMP6 treatment compared to sh-CTR. Data are shown as fold on respective untreated cells. (Figure 4.10 C).

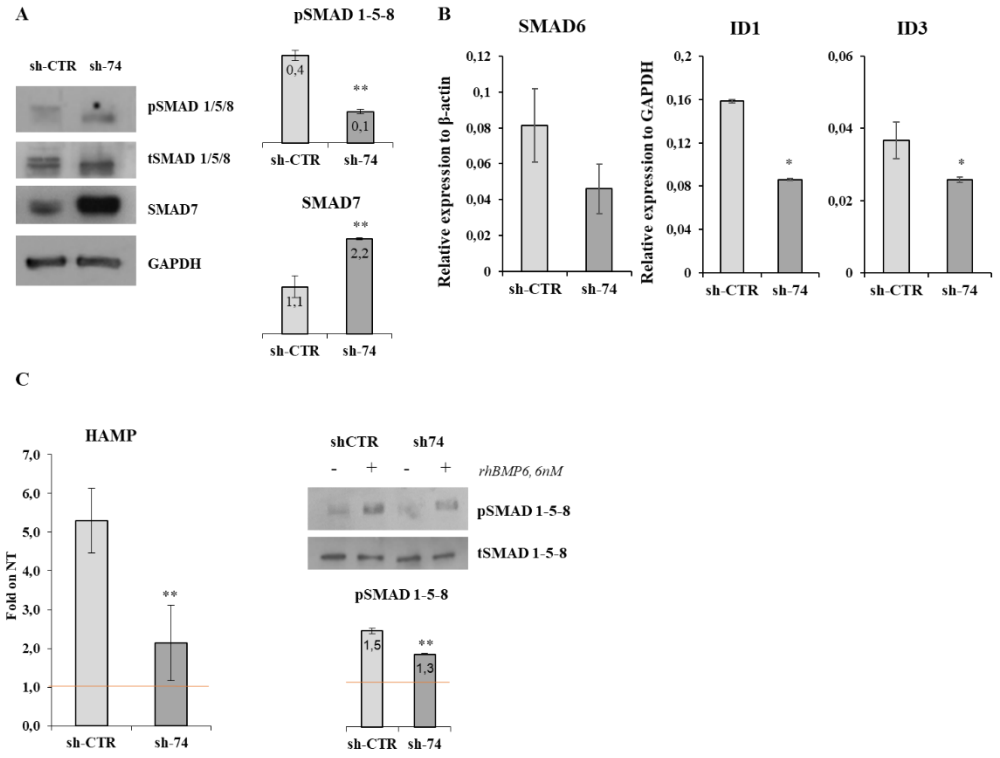

Figure 4.10. Evaluation of BMP/SMAD pathway in *SEC23B*-silenced Huh7. A. (Left panel) Representative immunoblots of pSMAD1-5-8, tSMAD 1-5-8 and SMAD7 proteins in total cells lysate of control Huh7 and sh74-*SEC23B* Huh7. GAPDH is the loading control. **(Right panel)** Quantification by densitometric analysis of three separate Western blots with similar results. Data are means ± standard deviation (**p < 0.01 vs. shCTR) **B**. Quantification of *SMAD6*, (normalized to *β-actin), ID1* and *ID3* (normalized to *GAPDH*, TaqMan assay) mRNA levels in control Huh7 and sh74-*SEC23B* Huh7. Data are means ± standard deviation of three independent experiments. (*p < 0.05, ** p< 0.01 vs. sh-CTR) **C. (Left panel)** Quantification of *HAMP* mRNA levels in control Huh7 and sh74-*SEC23B* Huh7 cells treated with rhBMP6, 2nM. Data are shown as fold on respective NT (red line) and are means ± standard deviation of three independent experiments. **(Right panel)** Representative immunoblots of pSMAD1-5-8 and tSMAD 1-5-8 proteins in total lysate of control Huh7 and sh74-*SEC23B* Huh7 cells treated (+) or not (-) with rhBMP6. Densitometric analysis of three separate Western blots with similar results is shown as fold on respective NT (red line)

4.10 Inhibition of glycosylation alters membrane proteins expression and hepatic iron metabolism

We further investigate the signaling pathway by assessing the protein expression of some components of the multiprotein membrane complex involved in BMP6 signaling. Particularly, we focused on TFR2, TMPRSS6, HFE and Hemojuvelin (HJV) whose protein expression resulted decreased in sh74-*SEC23B* cells compared to sh-CTR cells. (Figure 4.11 A).

To state the role of glycosylation in expression of these proteins, we treated Huh7 control cells with increasing concentrations of tunicamycin (0.5, 1.0, 1.5 µg/mL) to inhibit glycosylation. Firstly, we quantified expressions of membrane proteins TFR2, TMPRSS6, HFE in cells treated with tunicamycin compared to cells treated with DMSO (vehicle). We found that protein expression was reduced according to the increased concentration of tunicamycin (Figure 4.11 B). Moreover, we evaluated the BMP/SMAD in the same experimental condition and we found a strong reduction in phosphorylation and activation of the pathway after tunicamycin treatment (Figure 4.11 C, left panel). Finally, to confirm the inactivation of the hepcidin regulative pathway after tunicamycin treatment, we measured mRNA levels of *HAMP* in Huh7 cells treated with the maximum concentration of tunicamycin (1.5 µg/mL) and we confirmed a strongly significant reduction compared to *HAMP* expression in cells treated with vehicle (Figure 4.11 C, right panel).

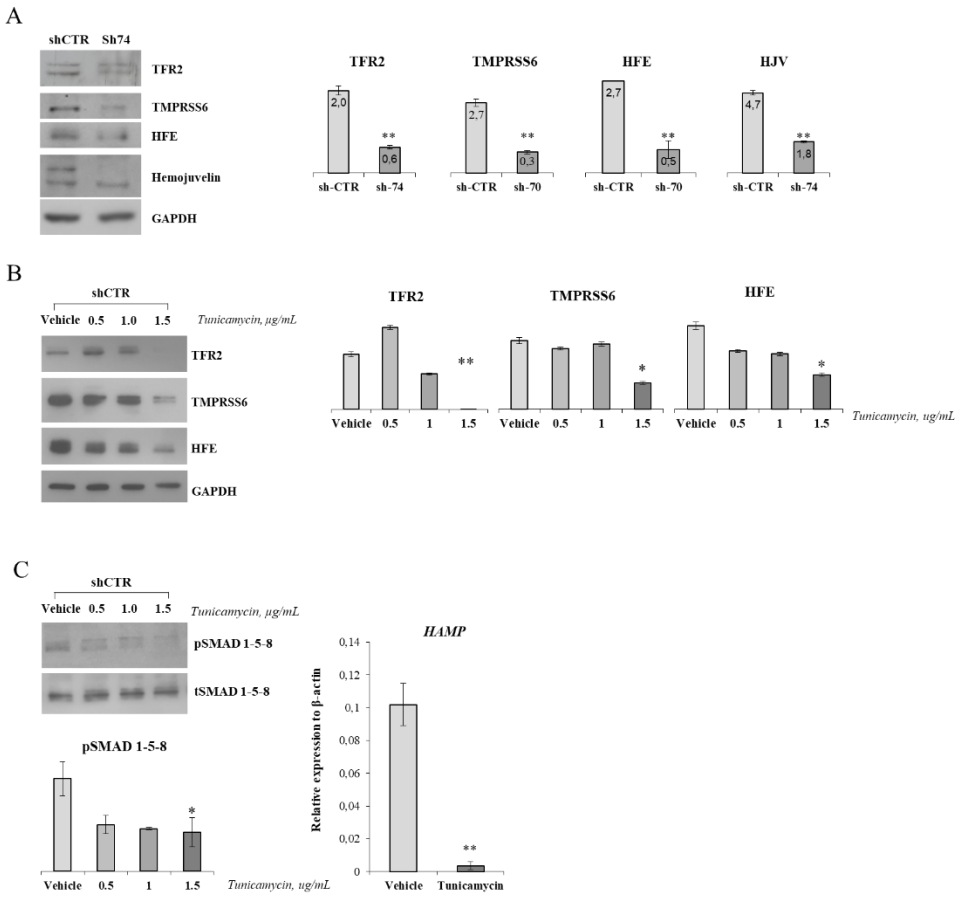

Figure 4.11. Analysis of the multiprotein membrane complex involved in BMP/SMAD pathway regulation and role of glycosylation in protein expression and pathway activation.

A. (Left panel) Representative immunoblots of TFR2, TMPRSS6, HFE and HJV proteins in total cells lysate of control Huh7 and sh74-*SEC23B* Huh7. GAPDH is the loading control. **(Right panel)** Quantification by densitometric analysis of three separate Western blots with similar results. Data are means ± standard deviation. (**p < 0.01 vs. shCTR) **B. (Left panel)** Representative immunoblots of TFR2, TMPRSS6, HFE in control Huh7 cells treated with DMSO (vehicle) or increasing concentration of tunicamycin (0.5, 1.0, 1.5 µg/mL). GAPDH is the loading control. **(Right panel)** Quantification by densitometric analysis of three separate Western blots with similar results. Data are means ± standard deviation. (*p < 0.05, **p < 0.01 of 1.5 µg/mL tunicamycin-treated cells vs DMSO-treated). **C. (Upper panel)** Representative immunoblots of pSMAD1-5-8 and tSMAD 1-5-8 proteins in control Huh7 cells treated with DMSO (vehicle) or increasing concentration of tunicamycin (0.5, 1.0, 1.5 µg/mL). **(Lower panel)** Quantification by densitometric analysis of three separate Western blots with similar results. Data are means ± standard deviation. (*p < 0.05, of 1.5 µg/mL tunicamycin-treated cells vs DMSO-treated). **(Right panel)** Quantification of *HAMP* mRNA levels, normalized to β-actin, in sh-CTR cells treated with DMSO and tunicamycin (1.5 µg/mL). Data are means ± standard deviation of three independent experiments. (**p < 0.01, vs vehicle treated cells).

4.11 *SEC23A* over-expression rescued iron overload in *SEC23B* silenced Huh7 cells.

Finally, we rescued the phenotype by over-expressing *SEC23A*, the *SEC23B* gene paralogue, in sh-74 Huh7 cells. This because *SEC23A* partially deputies *SEC23B* functions in patients with loss of function mutations in *SEC23B* (Tao et al. 2012). Lentiviral vector expresses SEC23A was transfected into sh-74 Huh7 cells for 24 and 48 hours. The over-expression of SEC23A was tested at both mRNA (Figure 4.12 A) and protein level (Figure 4.12 B). According to the transfection rate we performed further experiments on cells transfected for 48 hours. We tested whether the over-expressed *SEC23A* was able to restore the iron status and we found that *HAMP* gene expression resulted strongly increased compared to sh-74 untreated cells. (Figure 4.12 C, upper panel)

Moreover, the over-expression of *SEC23A* resulted in restored BMP-SMAD pathway, confirmed by the increased phosphorylation levels of SMAD 1-5-8 (Figure 4.12 D) and by increased *SMAD6* gene expression. (Figure 4.12 C, lower panel)

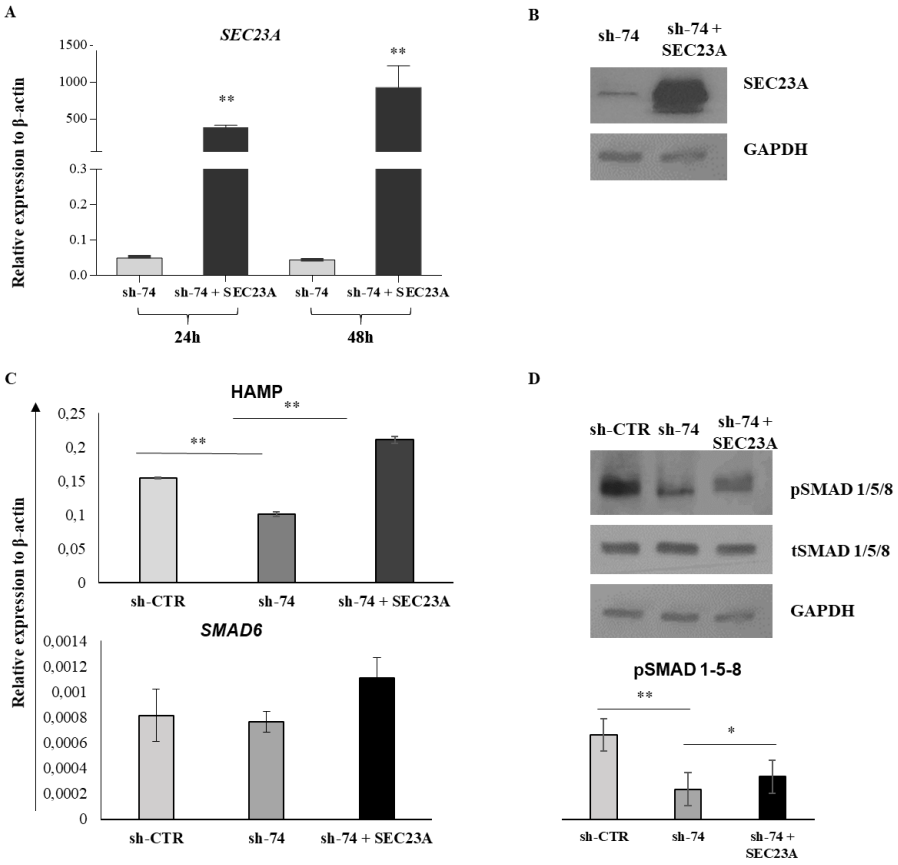

Figure 4.12: SEC23A over-expression rescued iron overload and restored BMP/SMAD pathway in *SEC23B* silenced Huh7 cells. A. Quantification of SEC23A mRNA levels normalized to β-actin in Huh7 cell line silenced for *SEC23B* (sh-74) or transfected with SEC23A (sh-74 + SEC23A) for 24 and 48 hours. Data are means ± standard deviation of three independent experiments. (**p < 0.01, vs relevant sh-74). **B.** Representative immunoblot of SEC23A and GAPDH in sh-74 cells and sh-74 transfected with SEC23A for 48h. **C.** Quantification of *HAMP* **(upper)** and *SMAD6* **(lower)** mRNA levels normalized to β-actin in sh-CTR, sh-74 and sh-74 transfected with SEC23A cells. **D. Upper panel.** Representative immunoblots showing pSMAD 1/5/8, tSMAD 1/5/8 and GAPDH as loading control of sh-CTR, sh-74 and sh-74 transfected with SEC23A cells. **Lower panel.** Quantification by densitometric analysis of three separate Western blots with similar results. Data are means ± standard deviation of three independent experiments. (*p< 0.05; **p < 0.01, sh74 vs sh-CTR and sh-74+SEC23A vs sh-74).

4.12 Inheritance of *SEC23B* and *PIEZO1* variants: proof of concept of iron overload linked to both the genes.

Within the large cohort of patients enrolled in our laboratory, we observed that a large percentage of patients with a conclusive diagnosis (17%) showed multilocus inheritance pattern. Of note, most patients with multilocus inheritance show a complex phenotype composed by DHS1 associated with HS or CDAs. Accordingly, *SEC23B*, *PIEZO1*, and *SPTA1* genes resulted the most frequently mutated gene among the HA-related genes. (Andolfo I, Martone S, et al., 2021) Among these patients, we focused on a clinical case referred by Hospital Galliera, Genova. The subject was a 32-years-old male who presented, at birth, hemolytic anemia, severe hepatic iron overload, jaundice, gallstones, and splenomegaly. First line investigations are summarized below (Table 1). The blood count (red) revealed a slightly reduced hemoglobin level, a mean corpuscular volume slightly increased and a relatively high reticulocyte count. In addition, biochemical data showed that hemolysis biomarkers (green) such as LDH and haptoglobin were positive. Moreover, a severe iron overload was stated by increased concentration of Ferritin, besides an increased percentage of transferrin saturation (dark red). (Table 1). The evaluation of family history highlighted that also the father suffered from anemia (Figure 4.13 A). Peripheral blood smear revealed the presence of stomatocytes up to 5% (Figure 4.13 B). The clinical case was finally evaluated by ektacytometry. The osmolarity curve was almost normal with only a slight alteration of DiMax (Figure 4.13 C). Finally, as third-line investigation, the proband was analyzed by targeted NGS. (Russo et al. 2018) Two pathogenetic variants have been found in both *SEC23B* and *PIEZO1* genes. In the first case, the variant was in homozygous state and was a transition c.325G>A, resulting in aminoacidic substitution p. Glu109Lys. The variant was reported as causative of CDA II with a minor allele frequency (MAF) of 0.0002 referring to 1000 genomes database. Besides, the *PIEZO1* variant is a heterozygous transition c.7505A>G, resulting in aminoacidic

replacement p. Lys2502Arg. *PIEZO1* variant was reported to be causative of DHS1 with a MAF = 0.002. The patient was finally diagnosed as a case of dual locus inheritance of DHS1 associated with CDAII.

Table 1. Laboratory data of the patient.

CBC	T.L. patient	Normal range
RBC (10^6/µl)	4.18	4.2-5.6
Hb (g/dl)	13.5	13-17.5
MCV (fl)	**98**	80-96
MCH (pg)	32.4	27-34
MCHC (g/dl)	33	32-37
Ret (%)	2.8	0.5-2
Ret (n.)	**117040**	-
RDW (%)	16.4	11-16
PLT (10^3µl)	199	150-450

Laboratory data	T.L. patient	Normal range
Total bilirubin (mg/dl)	**3.5**	0.2-1.1
Ind. bilirubin (mg/dl)	**2.6**	0.0-1.0
Serum iron (µg/dl)	**221**	45-150
Ferritin (ng/ml)	**1938**	5-150
Trasf. Sat (%)	**88**	15-45
LDH (IU/l)	**596**	227-450
Aptoglobin (g/l)	<3	0.6-3.6
AST (IU/l)	55	7-55 U/l
ALT (IU/l)	112	8-48 U/l

RBC, red blood cells; Hb, hemoglobin; MCV, mean corpuscular volume; MCH, mean corpuscular hemoglobin; MCHC, mean corpuscular hemoglobin concentration; Ret, reticulocytes; RDW, red blood cells distribution width; PLT, platelets; LDH; lactate dehydrogenase; AST, aspartate transaminase; ALT, alanine transaminase.

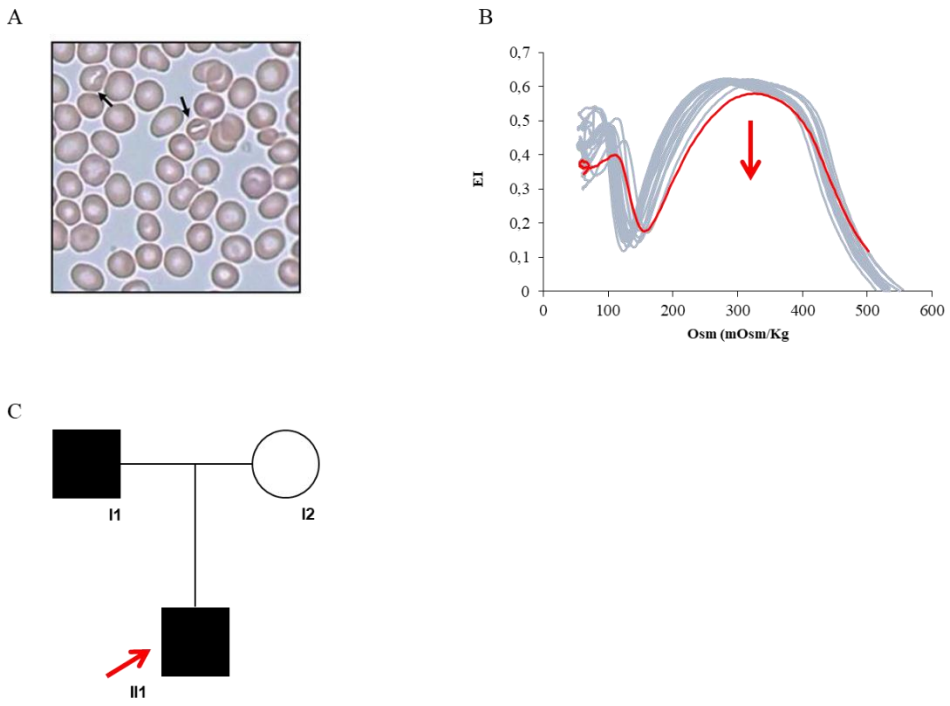

Figure 4.13. **Blood smear, ektacytometry curve and family pedigree**. **A.** Peripheral blood smear. Black arrows indicate stomatocytes. **B.** Ektacytometry curve of the proband (red curve) compared to healthy controls (blue curves). Alteration of DiMax showed by lowering of the curve peak. (red arrow) **C.** Family's pedigree. Squares denote male, circle females, solid symbols affected ones. The red arrow indicates proband.

5. Discussion

Hereditary hemolytic anemias are a group of heterogeneous disorders with clinical manifestations ranging from completely asymptomatic to life-threatening hemolytic anemia. Their genetic etiology includes mutations in genes that control RBCs production, structure, and function. The most common defects in these diseases occur in RBC membrane cytoskeleton genes, which weaken their structure and function (as dehydrated hereditary stomatocytosis). These are followed by defects in the globin genes, which lead to ineffective erythropoiesis and premature destruction of RBCs. Then, there are erythrocytic enzyme defects that decrease the RBC life span (i.e G6PD deficiency). Other rare hereditary anemias include congenital dyserythropoietic anemia and Diamond-Blackfan anemia which are primarily characterized by ineffective erythropoiesis. (Rets et al. 2019). The phenotypic presentations range from mild-to-severe with diverse complications. One of these complications is the iron overload.

This thesis project is focused on the molecular bases of iron overload in two different hereditary hemolytic anemias. Dehydrated hereditary stomatocytosis, belonging to the class of HHA due to RBCs membrane defects and Congenital dyserythropoietic anemia type II that is classified among the HHAs due to ineffective erythropoiesis. DHS is an autosomal dominant hemolytic anemia characterized by cation leak (particularly, cells lose K^+) that determines the dehydration of the red cells and that results in slightly increased MCV and MCHC. (Andolfo et al. 2016) On the other hand, CDAII is the most common form of CDAs, an heterogenous group of rare anemias characterized by defects in erythropoiesis. Both conditions present mild anemia and a slightly increased reticulocyte count. In both conditions the iron overload is the worst complication although the molecular bases are not well understood yet. Iron overload in DHS cannot be associated to the degree of anemia or to the transfusion regimen as well demonstrated in several genotype-phenotype correlation studies. (Andolfo, Russo, et al. 2018; Orvain et al. 2018; Picard et

al. 2019). On the contrary, the transfusion regimen and the hemolytic component can be strongly associated to iron loading conditions in CDAII patients. (Iolascon, Andolfo, and Russo 2020) This last has been associated to the over-production of specific erythroid regulators that suppress hepcidin, the master regulator of iron metabolism, leading to iron overload. The most representative hormone in this field is ERFE whose production is guided in turn by EPO, another hormone that reflects the need of iron in both physiological and pathological conditions. (Ganz and Nemeth 2012) To this aim, the first point of this project was the characterization of those regulators that take part in determining iron overload. Firstly, to state the iron overload in patients with DHS1 and CDAII, hepcidin was measured in plasma samples. Both cohorts of patients presented extremely low levels of hepcidin, referring to normal ranges. To determine whether hepcidin suppression was linked to alteration in erythroid compartment, ERFE levels in plasma samples of DHS and CDAII patients were quantified. Most of DHS1 patients presented almost normal or slightly increased levels in DHS1 confirming that a little alteration in erythropoiesis occurs, and accounts for ERFE over-production, although is not enough to explain the reduced hepcidin concentration. Besides, CDAII patients showed a more heterogeneous behavior. Even though the hormone resulted mainly up-regulated, as expected for an HHA characterized by ineffective erythropoiesis, several patients presented normal levels of ERFE. To understand this tendency, CDAII patients were further stratified basing on Hb levels. Patients with severe anemia (Hb < 10.5 g/dL, n= 41) presented higher level of ERFE compared to patients with Hb levels > 10.5 g/dL (n= 14) although correlation remains ambiguous. Of note, correlation of hepcidin and ERFE levels confirmed that alterations in ERFE production cannot fully explain the reduced hepcidin. This data suggested two observations: i) iron overload in DHS patients is associated to a non-erythroid dependent mechanism; ii) an amount of mildly affected CDAII patients presents iron overload regardless normal levels of ERFE. For this reason, we hypothesized a

specific role of *PIEZO1* and *SEC23B* genes, at hepatic level, in determining iron overload. *PIEZO1* is the first causative gene of DHS1, and its pathological mechanism is associated to alterations in the kinetics of ion channels that resulted in increased intracellular Ca^{2+} and decreased intracellular K^{+} in RBCs. Firstly, liver expression level of PIEZO1 and its role in physiological condition were determined. We observed high expression of the channel in several tissues, including liver. Considering that, we measured mRNA and protein expression in three different hepatic cell lines: Huh7, a hepatoma cell line, HepG2 that derives from hepatocellular carcinoma, and HepaRG as human hepatocyte. All three cell lines presented high expression of PIEZO1 at both protein and mRNA level. HepG2 cell line was excluded from further analysis as it represented a more undifferentiated model. Basing on this data, we tested the physiological role of PIEZO1 in liver. PIEZO1 was chemically activated (as the mechanoreceptor requires activation) with Yoda-1 molecule that acts as agonist (Syeda et al. 2015) or inhibited with its selective inhibitor, GsMTx-4. (Gnanasambandam et al. 2017) Firstly, we measured intracellular calcium concentration in untreated, activated, and inhibited cells, and we observed, as expected, that the activation of the channel induced a significant increase in intracellular calcium content compared to untreated cells in both cell systems. On the contrary, the inhibition of PIEZO1 blocked the intake of calcium. Finally, we tested whether activation or blocking of PIEZO1 at hepatic level was related to *HAMP* regulation. We observed, in both cell lines, that Yoda-1 mediated activation led to a strong reduction in hepcidin mRNA level that was restored after inhibition of PIEZO1. This data confirmed the hypothesis that a specific role of PIEZO1 at hepatic level accounts for iron overload. To study how PIEZO1 is integrated in the complex landscape of iron metabolism, we created a cellular hepatic model overexpressing in Huh7 cells two point GoF mutations: p.R2456H, the most frequent mutation reported in DHS1 patient, (Andolfo, Russo, et al. 2018) and p. R2488Q that we found in a family that showed a severe iron overload. Both PIEZO1 variants localized in the

intracellular C-terminal domain of PIEZO1. Interestingly, most of DHS patients presenting a severer iron overload carry mutations in the pore domain of PIEZO1, which is responsible for the ion passage. Conversely, most of the patients mildly affected by DHS1 show mutations in the non-pore domain, which is responsible for the mechanosensitive properties of the channel. (Andolfo, Russo, et al. 2018) The effect of the mutations was tested by evaluating *HAMP* gene expression, in cells previously treated with PIEZO1 activator, that resulted significantly reduced in both mutants and testing their ability to pass calcium. Gain of function mutations in PIEZO1 have been already reported to increase intracellular calcium concentration in RBCs (Glogowska et al. 2017; Gudipaty et al. 2017) and this was confirmed in our hepatic system where we observed an increase in calcium intake in cells overexpressing the two mutations, and restored in cells treated with GsMTx-4. To assess the link between altered intracellular calcium levels and unbalanced hepcidin expression we reproduced the calcium increase guided by PIEZO1, overloading untreated cells with Ca^{2+} ionophore A23187. Indeed, calcium overload strongly reduced *HAMP* gene expression, confirming the assessment. Stating that, we hypothesized that the role of PIEZO1 in iron overload could be associated to the PIEZO1-Ca^{2+}-triggered ERK1/2 signaling. (Cahalan et al. 2015; Liang et al. 2017) We, then, focused on the alteration of two intracellular pathways: MAPK pathway, that have been already reported associated to PIEZO1, (Piddini 2017) and BMP/SMADs pathway, the main hepatic iron regulative pathway. (Silvestri et al. 2019). In our system we observed that the ERK 1/2 pathway was hyper-activated compared to WT, while the BMP/SMADs pathway appeared to be downregulated. Of note, there are several evidences of the interplay of these two pathways. (Itoh et al. 2000; Luo 2017). Most of these mechanisms regard the phosphorylation of the SMADs (particularly SMAD1) in their linker region, thus sequestering the R-SMAD complex in the cytoplasm and promoting its degradation. (Sangkhae and Nemeth 2019) At the same time, ERK1/2-mediated BMP/SMADs regulation is

reported to involve SMAD7 transcription (Brodin et al. 2000) and SMAD4 degradation. (Liang et al. 2004) Indeed, to confirm the relation of these two pathways in our cellular model we treated cells with PD0325901, a potent inhibitor of ERK1/2 phosphorylation, and we confirmed that the reduced phosphorylation of ERK1/2 led to a consequent increase in phosphorylation levels of SMAD1/5/8. The altered BMP/SMAD pathway was further investigated analyzing mRNA levels of some target genes, *SMAD6, SMAD7*, *ID1,* and *ID3* that were all reduced. There were also reduced mRNA and protein levels of TMPRSS6, another membrane protein essential for systemic iron homeostasis that is indirectly regulated by the BMP/SMADs pathway, through *ID1*. (Meynard et al. 2011) The strong link between the *PIEZO1* mutations and the impairment of these intracellular pathways has been established by the inhibition of PIEZO1. We demonstrated that the PIEZO1 inhibitor, GsMTx-4, completely rescued ERK1/2 activation and SMAD1/5/8 inhibition. According to these data, we also showed that *HAMP* and *ID1* expression were restored to WT levels in the *PIEZO1* mutants after GsMTx-4 treatment. All these data confirm the determinant role of PIEZO1 as new iron regulator. Nevertheless, a transient model represents a strong limit to investigate a complex scenario as the one of iron systemic homeostasis. To overcome the lack of a more consistent model, we created a cellular hepatic system modified by the means of CRISPR-CAS9 technology with the variant c.7367 G>A, p.R2456H in heterozygous state. As expected, the gain of function mutation does not alter *PIEZO1* expression but impairs the cation flux. (Andolfo et al. 2013) Indeed, an increase in potassium channel activity and in intracellular calcium concentration in PIEZO1_KI cells were observed. Moreover, the unbalanced iron metabolism was confirmed by firstly analyzing the strong reduction of *HAMP* gene expression in KI cells and secondarily stating the alteration of the BMP/SMAD. Both target genes expression (*SMAD6, ID1)* and phosphorylation levels of SMAD 1/5/8 resulted downregulated in KI compared to WT. The convenience of this model led

multiple "-omics" approaches to extend pathway analyses. Indeed, we performed proteomics and transcriptomics analyses. Results from RNA sequencing are not shown in this work as they have been obtained only recently. Anyway, preliminary data confirmed the impairment of genes previously analyzed. The "big data" obtained are still far from a full comprehension, but several important issues came out. Although the proteome is extremely dynamic and depends on several conditions, we highlighted the de-regulation of diverse pathways. Beyond the vague and ambiguous "Metabolic pathways" classification, that comprehends the majority of proteins (15% of significantly up-regulated proteins), we focused on proteins belonging to the "Regulation of actin cytoskeleton pathway". Particularly, we found an increase in MAP2K1 (MEK1) and RRAS protein, firstly demonstrating that MAPK pathway alteration could start up-streamer than ERK1/2. This observation was confirmed by the increased expression of IQGAP3 protein. IQGAP3 is a Ras GTPase-activating-like (GAP) protein that is involved in cell-cell contacts of hepatocytes and acts at the interface between cytoskeleton and the cellular signaling as it regulates Ras/ERK cascade. (Kunimoto et al. 2009) Moreover, through IQ-motifs, located towards the middle of the primary sequence, can bind the calcium-sensing protein calmodulin. (Atcheson et al. 2011) Another interesting protein found was the Rho-GAP protein, ARHGAP35. This protein was reported, by similarity with mouse protein, to be involved in signal transduction of p21-ras to the nucleus, acting via Ras-GAPs. (Bradley et al. 2006). An important feature of this protein is its regulation that mainly requires phosphorylation by protein kinase C alpha (PRKCA) (Levay, Settleman, and Ligeti 2009). Although not present in filtered data (excluded as not significant), we analyzed raw data of PRKCA protein expression, observing an up-regulation in PIEZO1_KI cells compared to PIEZO1_WT. As widely known, PKRCA is a calcium-activated serine/threonine-protein kinase representing another proof of concept of the link between calcium and altered MAPK pathway. Our proposed model is summarized in Figure 5.1

The complex scene of hepatic iron metabolism was investigated to elucidate the iron loading in patients with CDAII, where the erythroid involvement cannot fully explain the hepcidin down regulation. We hypothesized a direct role of *SEC23B*, the causative gene of CDAII. SEC23B is a component of the COPII complex and is involved in secretory pathway of eukaryotic cells mediating anterograde transport of correctly folded cargo from the ER toward the Golgi apparatus.

We established a Huh7 cell model stably silenced for the *SEC23B* gene by two different lentivirals shRNAmir targeting human *SEC23B*, named sh-70 and sh-74. We firstly tested the efficiency of the silencing for both sh-70 and sh-74 by analyzing gene and protein expression of SEC23B itself and its paralogue SEC23A. Both models were positive for *SEC23B* silencing. On the contrary, we observed a significant downregulation of SEC23A in the Huh7 sh-*SEC23B*-70 cells suggesting a less-specific effect of the silencing in the Huh7 sh-*SEC23B*-70 cells. For this reason, further analyses were performed only on Huh7 sh-*SEC23B*-74 cells. As starting point, we evaluated the iron status of Huh7 sh-*SEC23B*-74 cells, in terms of *HAMP* and *Ferritin* expression. *HAMP* expression was found strongly reduced, confirming *ex vivo* data. On the other hand, Ferritin resulted up-regulated for both mRNA and protein expression. To explain the reduction in *HAMP* gene expression, we measured the activation of the main pathway involved in hepcidin regulation, the BMP/SMAD pathway. At protein level we observed a reduction in phosphorylation levels of SMAD 1-5-8 and the activation of the SMADs inhibitor, SMAD7 protein. The inactivation of the pathway was confirmed by the analysis of mRNA levels of BMP target genes as *SMAD6, ID1* and *ID3* that presented a strongly reduced expression. As proof of concept, we tested the efficiency of Huh7 sh-*SEC23B*-74 cells in activating the pathway after BMP6 stimulation. Surprisingly, we observed that Huh7 sh-*SEC23B*-74 cells presented a reduced ability to respond to BMP6 stimulation leading to a reduced activation of SMAD 1-5-8 phosphorylation and in turn to *HAMP* transcription. This data suggested that

SEC23B silenced cells failed to transduce external stimuli inside the cytoplasm. The link between the extracellular BMP6-dependent signal and the activation of pSMAD 1-5-8 requires the assembly of a multiprotein complex that senses and regulate the pathway. (D'Alessio, Hentze, and Muckenthaler 2012) The hereditary hemochromatosis-associated membrane proteins HFE, TFR2, and HJV are required for adequate hepatic expression of the iron hormone hepcidin. (Gao et al. 2009; Schmidt, Andrews, and Fleming 2010; Wallace et al. 2009) Besides, TMPRSS6 protein accounts for negative regulation of the pathway by the cleavage of HJV. (Silvestri et al. 2009; Silvestri et al. 2008) In our *in-vitro* system silenced for *SEC23B*, all these proteins were found to be down-regulated compared to control cells. These proteins have in common the complex post-translational modification that requires N-glycosylation for the correct localization (HFE), activation (TMPRSS6) and stabilization (TFR2). (Bhatt et al. 2010; Jiang et al. 2014; Zhao and Enns 2013). Treatment with increasing concentrations of tunicamycin, a potent N-linked glycosylation inhibitor, (Salzberger et al. 2015) confirmed that the altered glycosylation led to a reduced expression of TFR2, HFE, TMPRSS6 proteins. Furthermore, we tested for the SMAD 1-5-8 phosphorylation status that resulted reduced according to increasing concentrations of tunicamycin and according to the reduction of the membrane proteins activating the pathway. These data were confirmed by the strong reduction in *HAMP* gene expression in cells treated with tunicamycin, suggesting that altered glycosylation is directly involved in regulation of hepatic iron metabolism. Taking together this data, we confirmed that the alteration of glycosylation pathway led to altered expression of membrane proteins that, in turns, failed to sense extracellular iron and to activate the intracellular regulatory pathway. (Figure 5.2) As proof of concept, we over-expressed *SEC23A* to vicariate the loss of *SEC23B* in sh74-cells and we observed that the iron overload was completely rescued as reported by the increased expression of *HAMP* mRNA levels, and of pSMAD 1/5/8 protein. Indeed, all target genes were upregulated in cells overexpressing *SEC23A.* This

finally confirm that the loss of *SEC23B* at hepatic level specifically accounts for iron balance deregulation.

We demonstrated that, although through different mechanisms, DHS1 and CDAII share the alteration in the SMADs signaling, leading to reduction in hepcidin production at hepatic level. As proof of this findings, a clinical case was here reported. This patient, referred to us from the Hospital Galliera of Genova, presented congenital hemolytic anemia with sever hepatic iron overload. Although the first findings guided the diagnosis to DHS, targeted-NGS revealed the presence of two pathogenetic variants: a homozygous mutation in *SEC23B* (c.325 G>A; p. Glu109Lys) and a heterozygous one in *PIEZO1* gene (c.7505A>G; p. Lys2502Arg). Both variants were reported to be causative of CDAII and DHS1 respectively. The patient was finally diagnosed as a case of digenic inheritance. The presence of both mutations clarified not only the hematological features but also justify the strong iron overload that is the result of an extremely strong downregulation of hepcidin production due to the additive effect of both genes.

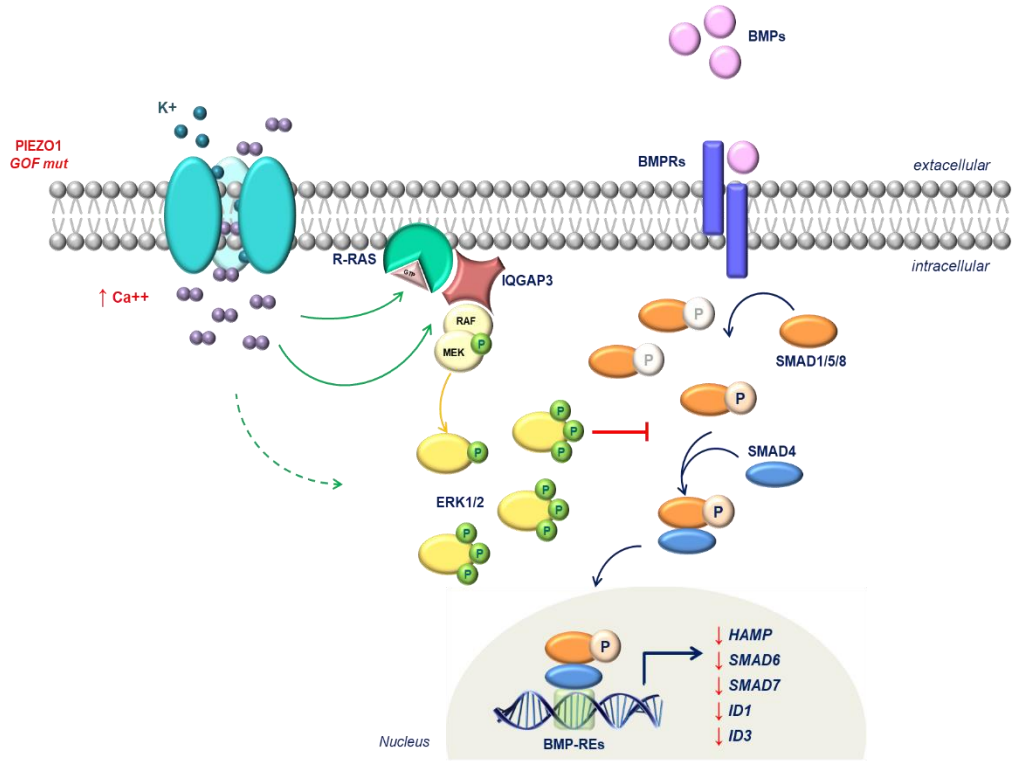

Figure 5.1. Schematic models of the pathogenic mechanisms of iron overload in patients with DHS1 *PIEZO1* gain-of-function (GoF) mutations results in increased intracellular Ca^{2+} concentrations. The hyperactivation of the mechanoreceptor leads to the activation of the MAPK pathway resulting in amplification of the phosphorylation of ERK1/2, which acts in turn by inhibiting the BMP/SMADs pathway. The lack of phosphorylation of SMAD1/5/8 inactivates transcription of target genes particularly *HAMP*

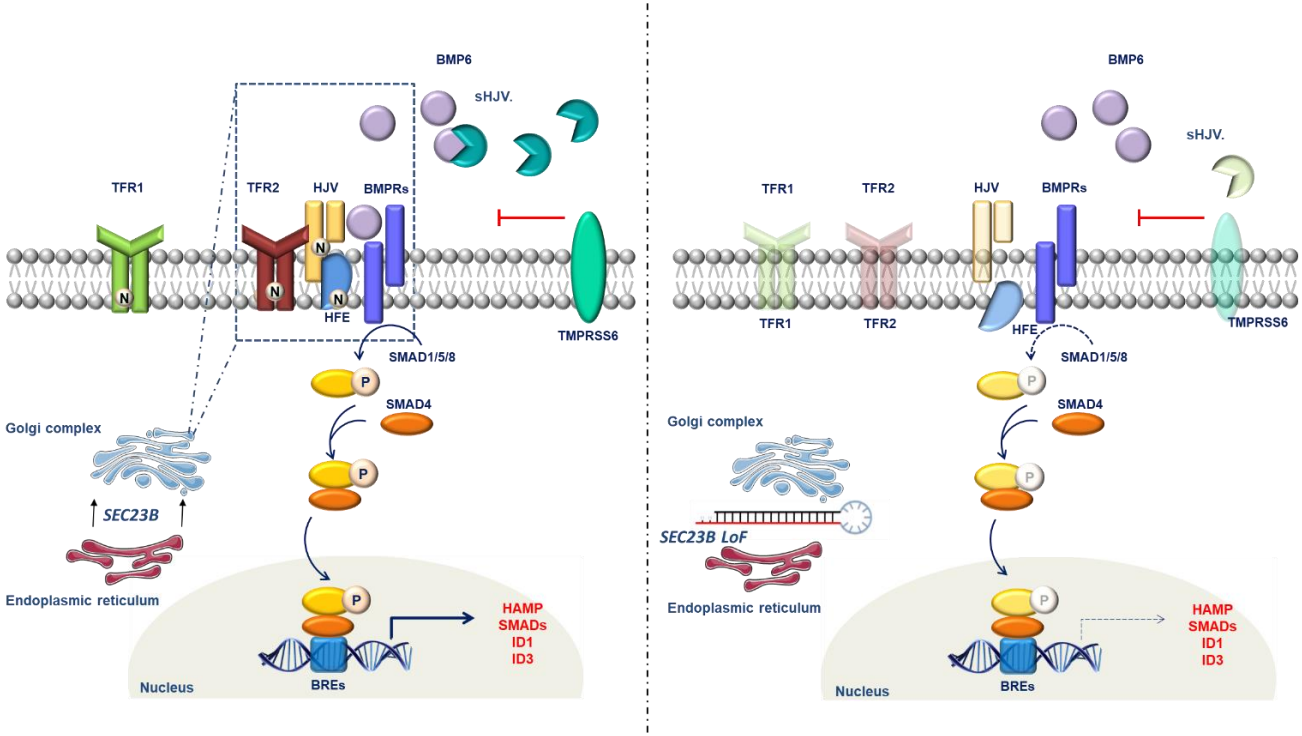

Figure 5.2: Figure 5. Schematic models of the pathogenic mechanisms of iron overload in patients with CDAII. **Left panel:** At physiological conditions, SEC23B mediates the anterograde trafficking of correctly folded proteins and post- translational modification. Correctly processed proteins (TFR2, HJV, HFE) associated in the membrane complex (dashed square) that mediates activation of BMP/SMAD pathway. This results in activation of BMP target genes, particularly hepcidin. **Right panel**: *SEC23B* loss of function determines the reduced expression of membrane proteins (light colored) preventing the stabilization of the complex. BMP6 failed to activate the pathway and this results in blocked *HAMP* transcription.

6. Conclusion

Iron overload represents the worst complications in patients with hereditary hemolytic anemias. Although iron metabolism requires a systemic and complex regulation that would be fully understand through animal models, to the best of our knowledge, this is the first demonstration of a specific role of *PIEZO1* and *SEC23B* in hepatic iron overload. Our findings could explain all the cases of iron overload in presence of mild anemia in DHS and CDAII. Affecting the main regulative pathway of hepatic iron metabolism, although through different mechanism, the two genes blocked the hepcidin production inducing iron overload. The involvement of the same pathway explains why the co-inheritance of mutations in both genes induces a more severe iron overload in the patient here analyzed. Regarding PIEZO1, this is the first demonstration of a link between alterations in cation channel and iron metabolism. Proteomic and transcriptomic data give us the opportunity to improve our knowledge identifying new actors in the complex landscape of iron metabolism. Studies on animal model have been already planned to understand how PIEZO1 could be inserted in a systemic scenario. On the other hand, we demonstrated that the impairment of glycosylation and in general of post-translational modifications pathway, due to *SEC23B* loss of function, is linked to the altered function of the membrane complex that transduces extracellular stimuli inside the cells through BMP/SMADs. We are now further elucidating the glycosylation mechanisms deregulated in *SEC23B* silenced cells and its final effect on iron metabolism. Despite the recent advances in the understanding of pathogenic mechanisms of DHS and CDAII, therapies are still lacking and DHS/CDAII clinical management is mainly based on supportive care. For this reason, understanding the molecular mechanism that underlie hepatic iron overload will be useful to shed light on new therapeutic strategies to treat the worst clinical complication in DHS and CDAII as in other iron-loading diseases characterized by possible similar alterations in PIEZO1 and SEC23B (such as thalassemia and sickle cells disease).

7. Acknowledgment

Firstly, I want to thank professor Iolascon for giving me the opportunity to grow-up in his laboratory.

This thesis project would not exist without the presence of my co-tutor, dr./prof Andolfo who always helped and supported me since the very beginning of my "career".

I also would like to express all my gratitude to prof. R. Russo who guided and encouraged me, during these years, to be always better and open-minded.

To the best mate I could ever wish for. I really want to thank my indispensable Ro(bertuccia) for turning every sad or difficult moment in laugh and madness.

Thanks to all my colleagues of Lab3 at CEINGE for the all-day-life, beyond the work.

To my family, the essential part of me.

To my lovely boyfriend, who is still with me although nobody understand how it can be possible. Thanks to remain by my side in good and bad times.

8. List of publications

1. Russo R, Marra R, **Rosato BE**, Iolascon A, Andolfo I. Genetics and Genomics Approaches for Diagnosis and Research into Hereditary Anemias. Front Physiol. 2020 Dec 22; 11:613559. doi: 10.3389/fphys.2020.613559. PMID: 33414725; PMCID: PMC7783452.
2. Russo R, Marra R, Andolfo I, Manna F, De Rosa G, **Rosato BE**, Radhakrishnan K,Fahey M, Iolascon A. Uridine treatment normalizes the congenital dyserythropoietic anemia type II-like hematological phenotype in a patient with homozygous mutation in the CAD gene. Am J Hematol. 2020 Nov;95(11): 1423-1426.doi: 10.1002/ajh.25946. Epub 2020 Aug 19. PMID: 32720728.
3. Russo R, Marra R, Andolfo I, De Rosa G, **Rosato BE**, Manna F, Gambale A, Raia M, Unal S, Barella S, Iolascon A. Characterization of Two Cases of Congenital Dyserythropoietic Anemia Type I Shed Light on the Uncharacterized C15orf41 Protein. Front Physiol. 2019 May 22; 10:621. doi: 10.3389/fphys.2019.00621. Erratum in: Front Physiol. 2020 Aug 11; 11:940. PMID: 31191338; PMCID: PMC6539198.
4. De Rosa G, Andolfo I, Marra R, Manna F, **Rosato BE**, Iolascon A, Russo R. RAP-011 Rescues the Disease Phenotype in a Cellular Model of Congenital Dyserythropoietic Anemia Type II by Inhibiting the SMAD2-3 Pathway. Int J Mol Sci. 2020 Aug 4;21(15):5577. doi: 10.3390/ijms21155577. PMID: 32759740; PMCID: PMC7432210.
5. Andolfo I, Lasorsa VA, Manna F, **Rosato BE**, Formicola D, Iolascon A, Capasso M. Kinome multigenic panel identified novel druggable EPHB4-V871I somatic variant in high-risk neuroblastoma. J Cell Mol Med. 2020 Jun;24(11): 6459-6471.doi: 10.1111/jcmm.15297. Epub 2020 Apr 26. PMID: 32336043; PMCID: PMC7294133.
6. Andolfo I, **Rosato BE**, Manna F, De Rosa G, Marra R, Gambale A, Girelli D, Russo R, Iolascon A. Gain-of-function mutations in *PIEZO1*

directly impair hepatic iron metabolism via the inhibition of the BMP/SMADs pathway. Am JHematol. 2020 Feb;95(2):188-197. doi: 10.1002/ajh.25683. Epub 2019 Dec 9. PMID:31737919.

7. Andolfo I, **Rosato BE**, Marra R, De Rosa G, Manna F, Gambale A, Iolascon A, Russo R. The BMP-SMAD pathway mediates the impaired hepatic iron metabolism associated with the ERFE-A260S variant. Am J Hematol. 2019 Nov;94(11): 1227-1235.doi: 10.1002/ajh.25613. Epub 2019 Aug 30. PMID: 31400017.
8. Andolfo I, De Rosa G, Errichiello E, Manna F, **Rosato BE**, Gambale A, Vetro A,Calcaterra V, Pelizzo G, De Franceschi L, Zuffardi O, Russo R, Iolascon A. *PIEZO1* Hypomorphic Variants in Congenital Lymphatic Dysplasia Cause Shape and Hydration Alterations of Red Blood Cells. Front Physiol. 2019 Mar 15;10: 258.doi: 10.3389/fphys.2019.00258. PMID: 30930797; PMCID: PMC6428731.
9. Andolfo I, Russo R, **Rosato BE**, Manna F, Gambale A, Brugnara C, Iolascon A. Genotype-phenotype correlation and risk stratification in a cohort of 123 hereditary stomatocytosis patients. Am J Hematol. 2018 Dec;93(12):1509-1517. doi: 10.1002/ajh.25276. Epub 2018 Oct 2. PMID: 30187933.
10. Russo R, Andolfo I, Manna F, Gambale A, Marra R, **Rosato BE**, Caforio P, Pinto V, Pignataro P, Radhakrishnan K, Unal S, Tomaiuolo G, Forni GL, Iolascon A. Multi-gene panel testing improves diagnosis and management of patients with hereditary anemias. Am J Hematol. 2018 May;93(5):672-682. doi: 10.1002/ajh.25058. Epub 2018 Feb 24. PMID: 29396846.
11. Andolfo I, Manna F, De Rosa G, **Rosato BE**, Gambale A, Tomaiuolo G, Carciati A, Marra R, De Franceschi L, Iolascon A, Russo R. *PIEZO1*-R1864H rare variant accounts for a genetic phenotype-modifier role in dehydrated hereditary stomatocytosis. Haematologica.

2018 Mar;103(3):e94-e97. doi: 10.3324/haematol.2017.180687. Epub 2017 Nov 30. PMID: 29191841; PMCID: PMC5830381.

Under Revision

1. Andolfo I, Martone S, **Rosato BE**, Marra R, Gambale A, Forni G, Pinto V, Göransson M, Vasiliki P, Gavillet M, Elalfy M, Panarelli A, Tomaiuolo G, Iolascon A and Russo R. Complex modes of inheritance in hereditary red blood cell disorders: a case series study of 155 patients. Am. J.Hematol.
2. Andolfo I, Russo R, Lasorsa VA, Cantalupo S, **Rosato BE**, Bonfiglio F, Frisso G, Abete P, Cassese G, Servillo G, Esposito G, Gentile I, Piscopo C, Villani R, Fiorentino G, Cerino P, Buonerba C, Pierri B, Zollo M, Iolasco A, Capasso M. Common variants at 21q22.3 locus influence MX1 gene expression and susceptibility to severe COVID-19. iScience

In preparation

1. *SEC23B* loss-of-function impairs iron metabolism by affecting glycosylation pathway in hepatic cells. **Rosato BE**, Andolfo I, Marra R, Manna F, Della Monica S, Martone S, Russo R and Iolascon A.
2. A knock-in PIEZO1-R2456H engineered hepatic cell line for the identification of novel players in iron overload. **Rosato BE***, Marra R*, Russo R, Iolascon A and. Andolfo I.

9. References

Aglialoro, F., N. Hofsink, M. Hofman, N. Brandhorst, and E. van den Akker. 2020. 'Inside Out Integrin Activation Mediated by PIEZO1 Signaling in Erythroblasts', *Front Physiol*, 11: 958.

Albuisson, J., S. E. Murthy, M. Bandell, B. Coste, H. Louis-Dit-Picard, J. Mathur, M. Feneant-Thibault, G. Tertian, J. P. de Jaureguiberry, P. Y. Syfuss, S. Cahalan, L. Garcon, F. Toutain, P. Simon Rohrlich, J. Delaunay, V. Picard, X. Jeunemaitre, and A. Patapoutian. 2013. 'Dehydrated hereditary stomatocytosis linked to gain-of-function mutations in mechanically activated PIEZO1 ion channels', *Nat Commun*, 4: 1884.

Andolfo I, Russo R, Iolascon A. Quando e come sospettare una patologia della membrana del globulo rosso. Ematologia pediatrica. 2014 Aprile-Giugno Vol. 44 N. 174 Pp.72-80

Andolfo, I., S. L. Alper, L. De Franceschi, C. Auriemma, R. Russo, L. De Falco, F. Vallefuoco, M. R. Esposito, D. H. Vandorpe, B. E. Shmukler, R. Narayan, D. Montanaro, M. D'Armiento, A. Vetro, I. Limongelli, O. Zuffardi, B. E. Glader, S. L. Schrier, C. Brugnara, G. W. Stewart, J. Delaunay, and A. Iolascon. 2013. 'Multiple clinical forms of dehydrated hereditary stomatocytosis arise from mutations in PIEZO1', *Blood*, 121: 3925-35, S1-12.

Andolfo, I., F. Manna, G. De Rosa, B. E. Rosato, A. Gambale, G. Tomaiuolo, A. Carciati, R. Marra, L. De Franceschi, A. Iolascon, and R. Russo. 2018. 'PIEZO1-R1864H rare variant accounts for a genetic phenotype-modifier role in dehydrated hereditary stomatocytosis', *Haematologica*, 103: e94-e97.

Andolfo, I., B. E. Rosato, R. Marra, G. De Rosa, F. Manna, A. Gambale, A. Iolascon, and R. Russo. 2019. 'The BMP-SMAD pathway mediates the impaired hepatic iron metabolism associated with the ERFE-A260S variant', *Am J Hematol*, 94: 1227-35.

Andolfo, I., R. Russo, A. Gambale, and A. Iolascon. 2016. 'New insights on hereditary erythrocyte membrane defects', *Haematologica*, 101: 1284-94.

Andolfo, I., R. Russo, F. Manna, B. E. Shmukler, A. Gambale, G. Vitiello, G. De Rosa, C. Brugnara, S. L. Alper, L. M. Snyder, and A. Iolascon. 2015. 'Novel Gardos channel mutations linked to dehydrated hereditary stomatocytosis (xerocytosis)', *Am J Hematol*, 90: 921-6.

Andolfo, I., R. Russo, B. E. Rosato, F. Manna, A. Gambale, C. Brugnara, and A. Iolascon. 2018. 'Genotype-phenotype correlation and risk stratification in a cohort of 123 hereditary stomatocytosis patients', *Am J Hematol*, 93: 1509-17.

Antonny, B., D. Madden, S. Hamamoto, L. Orci, and R. Schekman. 2001. 'Dynamics of the COPII coat with GTP and stable analogues', *Nat Cell Biol*, 3: 531-7.

Arezes, J., N. Foy, K. McHugh, A. Sawant, D. Quinkert, V. Terraube, A. Brinth, M. Tam, E. R. LaVallie, S. Taylor, A. E. Armitage, S. R. Pasricha, O. Cunningham, M. Lambert, S. J. Draper, R. Jasuja, and H. Drakesmith. 2018. 'Erythroferrone inhibits the induction of hepcidin by BMP6', *Blood*, 132: 1473-77.

Assis, R. A., C. Kassab, F. S. Seguro, F. F. Costa, P. A. Silveira, J. Wood, and N. Hamerschlak. 2013. 'Iron overload in a teenager with xerocytosis: the importance of nuclear magnetic resonance imaging', *Einstein (Sao Paulo)*, 11: 528-32.

Ataga, K. I., M. Reid, S. K. Ballas, Z. Yasin, C. Bigelow, L. S. James, W. R. Smith, F. Galacteros, A. Kutlar, J. H. Hull, J. W. Stocker, and I. C. A. Study Investigators. 2011. 'Improvements in haemolysis and indicators of erythrocyte survival do not correlate with acute vaso-occlusive crises in patients with sickle cell disease: a phase III randomized, placebo-controlled, double-blind study of the Gardos channel blocker senicapoc (ICA-17043)', *Br J Haematol*, 153: 92-104.

Atcheson, E., E. Hamilton, S. Pathmanathan, B. Greer, P. Harriott, and D. J. Timson. 2011. 'IQ-motif selectivity in human IQGAP2 and IQGAP3: binding of calmodulin and myosin essential light chain', *Biosci Rep*, 31: 371-9.

Babitt, J. L., F. W. Huang, D. M. Wrighting, Y. Xia, Y. Sidis, T. A. Samad, J. A. Campagna, R. T. Chung, A. L. Schneyer, C. J. Woolf, N. C. Andrews, and H. Y. Lin. 2006. 'Bone morphogenetic protein signaling by hemojuvelin regulates hepcidin expression', *Nat Genet*, 38: 531-9.

Badens, C., and H. Guizouarn. 2016. 'Advances in understanding the pathogenesis of the red cell volume disorders', *Br J Haematol*, 174: 674-85.

Bae, C., R. Gnanasambandam, C. Nicolai, F. Sachs, and P. A. Gottlieb. 2013. 'Xerocytosis is caused by mutations that alter the kinetics of the mechanosensitive channel PIEZO1', *Proc Natl Acad Sci U S A*, 110: E1162-8.

Barcellini, W., and B. Fattizzo. 2015. 'Clinical Applications of Hemolytic Markers in the Differential Diagnosis and Management of Hemolytic Anemia', *Dis Markers*, 2015: 635670.

Begenisich, T., T. Nakamoto, C. E. Ovitt, K. Nehrke, C. Brugnara, S. L. Alper, and J. E. Melvin. 2004. 'Physiological roles of the intermediate conductance, Ca2+-activated potassium channel Kcnn4', *J Biol Chem*, 279: 47681-7.

Bhatt, L., C. Murphy, L. S. O'Driscoll, M. Carmo-Fonseca, M. W. McCaffrey, and J. V. Fleming. 2010. 'N-glycosylation is important for the correct intracellular localization of HFE and its ability to decrease cell surface transferrin binding', *FEBS J*, 277: 3219-34.

Bradley, W. D., S. E. Hernandez, J. Settleman, and A. J. Koleske. 2006. 'Integrin signaling through Arg activates p190RhoGAP by promoting its binding to p120RasGAP and recruitment to the membrane', *Mol Biol Cell*, 17: 4827-36.

Brodin, G., A. Ahgren, P. ten Dijke, C. H. Heldin, and R. Heuchel. 2000. 'Efficient TGF-beta induction of the Smad7 gene requires cooperation between AP-1, Sp1, and Smad proteins on the mouse Smad7 promoter', *J Biol Chem*, 275: 29023-30.

Bruce, L. J. 2009. 'Hereditary stomatocytosis and cation-leaky red cells--recent developments', *Blood Cells Mol Dis*, 42: 216-22.

Cahalan, S. M., V. Lukacs, S. S. Ranade, S. Chien, M. Bandell, and A. Patapoutian. 2015. 'Piezo1 links mechanical forces to red blood cell volume', *Elife*, 4.

Cappellini, M. D., E. Grespi, E. Cassinerio, D. Bignamini, and G. Fiorelli. 2005. 'Coagulation and splenectomy: an overview', *Ann N Y Acad Sci*, 1054: 317-24.

Carella, M., G. Stewart, J. F. Ajetunmobi, S. Perrotta, S. Grootenboer, G. Tchernia, J. Delaunay, A. Totaro, L. Zelante, P. Gasparini, and A. Iolascon. 1998. 'Genomewide search for dehydrated hereditary stomatocytosis (hereditary xerocytosis): mapping of locus to chromosome 16 (16q23-qter)', *Am J Hum Genet*, 63: 810-6.

Carmona, U., L. Li, L. Zhang, and M. Knez. 2014. 'Ferritin light-chain subunits: key elements for the electron transfer across the protein cage', *Chem Commun (Camb)*, 50: 15358-61.

Casanovas, G., D. W. Swinkels, S. Altamura, K. Schwarz, C. M. Laarakkers, H. J. Gross, M. Wiesneth, H. Heimpel, and M. U. Muckenthaler. 2011. 'Growth differentiation factor 15 in patients with congenital dyserythropoietic anaemia (CDA) type II', *J Mol Med (Berl)*, 89: 811-6.

Casanovas, G., M. Vujic Spasic, C. Casu, S. Rivella, J. Strelau, K. Unsicker, and M. U. Muckenthaler. 2013. 'The murine growth differentiation factor 15 is not essential for systemic iron homeostasis in phlebotomized mice', *Haematologica*, 98: 444-7.

Caulier, A., N. Jankovsky, Y. Demont, H. Ouled-Haddou, J. Demagny, C. Guitton, L. Merlusca, D. Lebon, P. Vong, A. Aubry, A. Lahary, C. Rose, S. Greaume, E. Cardon, J. Platon, H. Ouadid-Ahidouch, J. Rochette, J. P. Marolleau, V. Picard, and L. Garcon. 2020. 'PIEZO1 activation delays erythroid differentiation of normal and hereditary xerocytosis-derived human progenitor cells', *Haematologica*, 105: 610-22.

Chen, H., Z. K. Attieh, B. A. Syed, Y. M. Kuo, V. Stevens, B. K. Fuqua, H. S. Andersen, C. E. Naylor, R. W. Evans, L. Gambling, R. Danzeisen, M.

Bacouri-Haidar, J. Usta, C. D. Vulpe, and H. J. McArdle. 2010. 'Identification of zyklopen, a new member of the vertebrate multicopper ferroxidase family, and characterization in rodents and human cells', *J Nutr*, 140: 1728-35.

Chen, X., S. Wanggou, A. Bodalia, M. Zhu, W. Dong, J. J. Fan, W. C. Yin, H. K. Min, M. Hu, D. Draghici, W. Dou, F. Li, F. J. Coutinho, H. Whetstone, M. M. Kushida, P. B. Dirks, Y. Song, C. C. Hui, Y. Sun, L. Y. Wang, X. Li, and X. Huang. 2018. 'A Feedforward Mechanism Mediated by Mechanosensitive Ion Channel PIEZO1 and Tissue Mechanics Promotes Glioma Aggression', *Neuron*, 100: 799-815 e7.

Core, A. B., S. Canali, and J. L. Babitt. 2014. 'Hemojuvelin and bone morphogenetic protein (BMP) signaling in iron homeostasis', *Front Pharmacol*, 5: 104.

Coste, B., S. E. Murthy, J. Mathur, M. Schmidt, Y. Mechioukhi, P. Delmas, and A. Patapoutian. 2015. 'Piezo1 ion channel pore properties are dictated by C-terminal region', *Nat Commun*, 6: 7223.

Crielaard, B. J., T. Lammers, and S. Rivella. 2017. 'Targeting iron metabolism in drug discovery and delivery', *Nat Rev Drug Discov*, 16: 400-23.

D'Alessio, F., M. W. Hentze, and M. U. Muckenthaler. 2012. 'The hemochromatosis proteins HFE, TfR2, and HJV form a membrane-associated protein complex for hepcidin regulation', *J Hepatol*, 57: 1052-60.

Da Costa, L., J. Galimand, O. Fenneteau, and N. Mohandas. 2013. 'Hereditary spherocytosis, elliptocytosis, and other red cell membrane disorders', *Blood Rev*, 27: 167-78.

De Franceschi, L., F. Turrini, E. M. del Giudice, S. Perrotta, O. Olivieri, R. Corrocher, F. Mannu, and A. Iolascon. 1998. 'Decreased band 3 anion transport activity and band 3 clusterization in congenital dyserythropoietic anemia type II', *Exp Hematol*, 26: 869-73.

Delaunay, J. 2004. 'The hereditary stomatocytoses: genetic disorders of the red cell membrane permeability to monovalent cations', *Semin Hematol*, 41: 165-72.

Dowdle, W. E., B. Nyfeler, J. Nagel, R. A. Elling, S. Liu, E. Triantafellow, S. Menon, Z. Wang, A. Honda, G. Pardee, J. Cantwell, C. Luu, I. Cornella-Taracido, E. Harrington, P. Fekkes, H. Lei, Q. Fang, M. E. Digan, D. Burdick, A. F. Powers, S. B. Helliwell, S. D'Aquin, J. Bastien, H. Wang, D. Wiederschain, J. Kuerth, P. Bergman, D. Schwalb, J. Thomas, S. Ugwonali, F. Harbinski, J. Tallarico, C. J. Wilson, V. E. Myer, J. A. Porter, D. E. Bussiere, P. M. Finan, M. A. Labow, X. Mao, L. G. Hamann, B. D. Manning, R. A. Valdez, T. Nicholson, M. Schirle, M. S. Knapp, E. P. Keaney, and L. O. Murphy. 2014. 'Selective VPS34 inhibitor blocks autophagy and uncovers a role for NCOA4 in ferritin degradation and iron homeostasis in vivo', *Nat Cell Biol*, 16: 1069-79.

Drakesmith, H., E. Nemeth, and T. Ganz. 2015. 'Ironing out Ferroportin', *Cell Metab*, 22: 777-87.

Faucherre, A., K. Kissa, J. Nargeot, M. E. Mangoni, and C. Jopling. 2014. 'Piezo1 plays a role in erythrocyte volume homeostasis', *Haematologica*, 99: 70-5.

Finberg, K. E., R. L. Whittlesey, M. D. Fleming, and N. C. Andrews. 2010. 'Down-regulation of Bmp/Smad signaling by Tmprss6 is required for maintenance of systemic iron homeostasis', *Blood*, 115: 3817-26.

Gallagher, P. G., S. H. Chang, M. P. Rettig, J. E. Neely, C. A. Hillery, B. D. Smith, and P. S. Low. 2003. 'Altered erythrocyte endothelial adherence and membrane phospholipid asymmetry in hereditary hydrocytosis', *Blood*, 101: 4625-7.

Gambale, A., A. Iolascon, I. Andolfo, and R. Russo. 2016. 'Diagnosis and management of congenital dyserythropoietic anemias', *Expert Rev Hematol*, 9: 283-96.

Ganz, T. 2013. 'Systemic iron homeostasis', *Physiol Rev*, 93: 1721-41.

Ganz, T., and E. Nemeth. 2012. 'Iron metabolism: interactions with normal and disordered erythropoiesis', *Cold Spring Harb Perspect Med*, 2: a011668.

Gao, J., J. Chen, M. Kramer, H. Tsukamoto, A. S. Zhang, and C. A. Enns. 2009. 'Interaction of the hereditary hemochromatosis protein HFE with transferrin receptor 2 is required for transferrin-induced hepcidin expression', *Cell Metab*, 9: 217-27.

Glogowska, E., K. Lezon-Geyda, Y. Maksimova, V. P. Schulz, and P. G. Gallagher. 2015. 'Mutations in the Gardos channel (KCNN4) are associated with hereditary xerocytosis', *Blood*, 126: 1281-4.

Glogowska, E., E. R. Schneider, Y. Maksimova, V. P. Schulz, K. Lezon-Geyda, J. Wu, K. Radhakrishnan, S. B. Keel, D. Mahoney, A. M. Freidmann, R. A. Altura, E. O. Gracheva, S. N. Bagriantsev, T. A. Kalfa, and P. G. Gallagher. 2017. 'Novel mechanisms of PIEZO1 dysfunction in hereditary xerocytosis', *Blood*, 130: 1845-56.

Gnanasambandam, R., C. Ghatak, A. Yasmann, K. Nishizawa, F. Sachs, A. S. Ladokhin, S. I. Sukharev, and T. M. Suchyna. 2017. 'GsMTx4: Mechanism of Inhibiting Mechanosensitive Ion Channels', *Biophys J*, 112: 31-45.

Grace, R. F., and B. Glader. 2018. 'Red Blood Cell Enzyme Disorders', *Pediatr Clin North Am*, 65: 579-95.

Grootenboer, S., P. O. Schischmanoff, I. Laurendeau, T. Cynober, G. Tchernia, J. P. Dommergues, D. Dhermy, M. Bost, B. Varet, M. Snyder, S. K. Ballas, B. Ducot, M. C. Babron, G. W. Stewart, P. Gasparini, A. Iolascon, and J. Delaunay. 2000. 'Pleiotropic syndrome of dehydrated hereditary stomatocytosis, pseudohyperkalemia, and perinatal edema maps to 16q23-q24', *Blood*, 96: 2599-605.

Gudipaty, S. A., J. Lindblom, P. D. Loftus, M. J. Redd, K. Edes, C. F. Davey, V. Krishnegowda, and J. Rosenblatt. 2017. 'Mechanical stretch triggers rapid epithelial cell division through Piezo1', *Nature*, 543: 118-21.

Hamdi, A., T. M. Roshan, T. M. Kahawita, A. B. Mason, A. D. Sheftel, and P. Ponka. 2016. 'Erythroid cell mitochondria receive endosomal iron by a "kiss-and-run" mechanism', *Biochim Biophys Acta*, 1863: 2859-67.

Hentze, M. W., M. U. Muckenthaler, B. Galy, and C. Camaschella. 2010. 'Two to tango: regulation of Mammalian iron metabolism', *Cell*, 142: 24-38.

Huang da, W., B. T. Sherman, and R. A. Lempicki. 2009. 'Bioinformatics enrichment tools: paths toward the comprehensive functional analysis of large gene lists', *Nucleic Acids Res*, 37: 1-13.

Iolascon, A., I. Andolfo, W. Barcellini, F. Corcione, L. Garcon, L. De Franceschi, C. Pignata, G. Graziadei, D. Pospisilova, D. C. Rees, M. de Montalembert, S. Rivella, A. Gambale, R. Russo, L. Ribeiro, J. Vives-Corrons, P. A. Martinez, A. Kattamis, B. Gulbis, M. D. Cappellini, I. Roberts, H. Tamary, Cells Working Study Group on Red, and E. H. A. Iron of the. 2017. 'Recommendations regarding splenectomy in hereditary hemolytic anemias', *Haematologica*, 102: 1304-13.

Iolascon, A., I. Andolfo, and R. Russo. 2019. 'Advances in understanding the pathogenesis of red cell membrane disorders', *Br J Haematol*, 187: 13-24.

Iolascon, A., I.Andolfo, and R.Russo. 2020. 'Congenital dyserythropoietic anemias', *Blood*, 136: 1274-83.

Iolascon, A., M. R. Esposito, and R. Russo. 2012. 'Clinical aspects and pathogenesis of congenital dyserythropoietic anemias: from morphology to molecular approach', *Haematologica*, 97: 1786-94.

Iolascon, A., H. Heimpel, A. Wahlin, and H. Tamary. 2013. 'Congenital dyserythropoietic anemias: molecular insights and diagnostic approach', *Blood*, 122: 2162-6.

Iolascon, A., R. Russo, M. R. Esposito, C. Piscopo, R. Asci, L. De Falco, and F. Di Noce. 2011. 'Congenital dyserythropoietic anaemias: new acquisitions', *Blood Transfus*, 9: 278-80.

Itoh, S., F. Itoh, M. J. Goumans, and P. Ten Dijke. 2000. 'Signaling of transforming growth factor-beta family members through Smad proteins', *Eur J Biochem*, 267: 6954-67.

Jiang, J., J. Yang, P. Feng, B. Zuo, N. Dong, Q. Wu, and Y. He. 2014. 'N-glycosylation is required for matriptase-2 autoactivation and ectodomain shedding', *J Biol Chem*, 289: 19500-7.

Kaufman, H. W., J. K. Niles, D. R. Gallagher, A. Rivera, S. L. Alper, C. Brugnara, and L. M. Snyder. 2018. 'Revised prevalence estimate of possible Hereditary Xerocytosis as derived from a large U.S. Laboratory database', *Am J Hematol*, 93: E9-E12.

Kautz, L., G. Jung, X. Du, V. Gabayan, J. Chapman, M. Nasoff, E. Nemeth, and T. Ganz. 2015. 'Erythroferrone contributes to hepcidin suppression and iron overload in a mouse model of beta-thalassemia', *Blood*, 126: 2031-7.

Kautz, L., G. Jung, E. V. Valore, S. Rivella, E. Nemeth, and T. Ganz. 2014. 'Identification of erythroferrone as an erythroid regulator of iron metabolism', *Nat Genet*, 46: 678-84.

Kautz, L., D. Meynard, A. Monnier, V. Darnaud, R. Bouvet, R. H. Wang, C. Deng, S. Vaulont, J. Mosser, H. Coppin, and M. P. Roth. 2008. 'Iron regulates phosphorylation of Smad1/5/8 and gene expression of Bmp6, Smad7, Id1, and Atoh8 in the mouse liver', *Blood*, 112: 1503-9.

Khoriaty, R., M. P. Vasievich, M. Jones, L. Everett, J. Chase, J. Tao, D. Siemieniak, B. Zhang, I. Maillard, and D. Ginsburg. 2014. 'Absence of a red blood cell phenotype in mice with hematopoietic deficiency of SEC23B', *Mol Cell Biol*, 34: 3721-34.

Kunimoto, K., H. Nojima, Y. Yamazaki, T. Yoshikawa, T. Okanoue, and S. Tsukita. 2009. 'Involvement of IQGAP3, a regulator of Ras/ERK-related cascade, in hepatocyte proliferation in mouse liver regeneration and development', *J Cell Physiol*, 220: 621-31.

Lanuti, P., V. Bertagnolo, A. R. Gaspari, F. Ciccocioppo, L. Pierdomenico, A. Bascelli, G. Sabatino, S. Miscia, and M. Marchisio. 2006. 'Parallel

regulation of PKC-alpha and PKC-delta characterizes the occurrence of erythroid differentiation from human primary hematopoietic progenitors', *Exp Hematol*, 34: 1624-34.

Levay, M., J. Settleman, and E. Ligeti. 2009. 'Regulation of the substrate preference of p190RhoGAP by protein kinase C-mediated phosphorylation of a phospholipid binding site', *Biochemistry*, 48: 8615-23.

Liang, J., B. Huang, G. Yuan, Y. Chen, F. Liang, H. Zeng, S. Zheng, L. Cao, D. Geng, and S. Zhou. 2017. 'Stretch-activated channel Piezo1 is up-regulated in failure heart and cardiomyocyte stimulated by AngII', *Am J Transl Res*, 9: 2945-55.

Liang, M., Y. Y. Liang, K. Wrighton, D. Ungermannova, X. P. Wang, F. C. Brunicardi, X. Liu, X. H. Feng, and X. Lin. 2004. 'Ubiquitination and proteolysis of cancer-derived Smad4 mutants by SCFSkp2', *Mol Cell Biol*, 24: 7524-37.

Lin, Y. C., Y. R. Guo, A. Miyagi, J. Levring, R. MacKinnon, and S. Scheuring. 2019. 'Force-induced conformational changes in PIEZO1', *Nature*, 573: 230-34.

Liu, G., S. Niu, A. Dong, H. Cai, G. J. Anderson, B. Han, and G. Nie. 2012. 'A Chinese family carrying novel mutations in SEC23B and HFE2, the genes responsible for congenital dyserythropoietic anaemia II (CDA II) and primary iron overload, respectively', *Br J Haematol*, 158: 143-5.

Lunde, N. N., M. H. Haugen, K. B. Bodin Larsen, I. Damgaard, S. J. Pettersen, R. Kasem, W. Rut, M. Drag, M. Poreba, H. T. Johansen, and R. Solberg. 2017. 'Glycosylation is important for legumain localization and processing to active forms but not for cystatin E/M inhibitory functions', *Biochimie*, 139: 27-37.

Luo, K. 2017. 'Signaling Cross Talk between TGF-beta/Smad and Other Signaling Pathways', *Cold Spring Harb Perspect Biol*, 9.

Maher, A. D., and P. W. Kuchel. 2003. 'The Gardos channel: a review of the Ca2+-activated K+ channel in human erythrocytes', *Int J Biochem Cell Biol*, 35: 1182-97.

Mariani, M., W. Barcellini, C. Vercellati, A. P. Marcello, E. Fermo, P. Pedotti, C. Boschetti, and A. Zanella. 2008. 'Clinical and hematologic features of 300 patients affected by hereditary spherocytosis grouped according to the type of the membrane protein defect', *Haematologica*, 93: 1310-7.

McHugh, B. J., A. Murdoch, C. Haslett, and T. Sethi. 2012. 'Loss of the integrin-activating transmembrane protein Fam38A (Piezo1) promotes a switch to a reduced integrin-dependent mode of cell migration', *PLoS One*, 7: e40346.

Meynard, D., V. Vaja, C. C. Sun, E. Corradini, S. Chen, C. Lopez-Otin, L. Grgurevic, C. C. Hong, M. Stirnberg, M. Gutschow, S. Vukicevic, J. L. Babitt, and H. Y. Lin. 2011. 'Regulation of TMPRSS6 by BMP6 and iron in human cells and mice', *Blood*, 118: 747-56.

Muckenthaler, M. U., S. Rivella, M. W. Hentze, and B. Galy. 2017. 'A Red Carpet for Iron Metabolism', *Cell*, 168: 344-61.

Nai, A., M. R. Lidonnici, M. Rausa, G. Mandelli, A. Pagani, L. Silvestri, G. Ferrari, and C. Camaschella. 2015. 'The second transferrin receptor regulates red blood cell production in mice', *Blood*, 125: 1170-9.

Ohgami, R. S., D. R. Campagna, E. L. Greer, B. Antiochos, A. McDonald, J. Chen, J. J. Sharp, Y. Fujiwara, J. E. Barker, and M. D. Fleming. 2005. 'Identification of a ferrireductase required for efficient transferrin-dependent iron uptake in erythroid cells', *Nat Genet*, 37: 1264-9.

Orvain, C., L. Da Costa, R. Van Wijk, S. Pissard, V. Picard, L. Mansour-Hendili, S. Cunat, M. Giansily-Blaizot, G. Cartron, J. F. Schved, and P. Aguilar-Martinez. 2018. 'Inherited or acquired modifiers of iron status may dramatically affect the phenotype in dehydrated hereditary stomatocytosis', *Eur J Haematol*, 101: 566-69.

Pagani, A., M. Vieillevoye, A. Nai, M. Rausa, M. Ladli, C. Lacombe, P. Mayeux, F. Verdier, C. Camaschella, and L. Silvestri. 2015. 'Regulation of cell surface transferrin receptor-2 by iron-dependent cleavage and release of a soluble form', *Haematologica*, 100: 458-65.

Papanikolaou, G., M. E. Samuels, E. H. Ludwig, M. L. MacDonald, P. L. Franchini, M. P. Dube, L. Andres, J. MacFarlane, N. Sakellaropoulos, M. Politou, E. Nemeth, J. Thompson, J. K. Risler, C. Zaborowska, R. Babakaiff, C. C. Radomski, T. D. Pape, O. Davidas, J. Christakis, P. Brissot, G. Lockitch, T. Ganz, M. R. Hayden, and Y. P. Goldberg. 2004. 'Mutations in HFE2 cause iron overload in chromosome 1q-linked juvenile hemochromatosis', *Nat Genet*, 36: 77-82.

Picard, V., C. Guitton, I. Thuret, C. Rose, L. Bendelac, K. Ghazal, P. Aguilar-Martinez, C. Badens, C. Barro, C. Beneteau, C. Berger, P. Cathebras, E. Deconinck, J. Delaunay, J. M. Durand, N. Firah, F. Galacteros, B. Godeau, X. Jais, J. P. de Jaureguiberry, C. Le Stradic, F. Lifermann, R. Maffre, G. Morin, J. Perrin, V. Proulle, M. Ruivard, F. Toutain, A. Lahary, and L. Garcon. 2019. 'Clinical and biological features in PIEZO1-hereditary xerocytosis and Gardos channelopathy: a retrospective series of 126 patients', *Haematologica*, 104: 1554-64.

Piddini, E. 2017. 'Epithelial Homeostasis: A Piezo of the Puzzle', *Curr Biol*, 27: R232-R34.

Porpiglia, E., D. Hidalgo, M. Koulnis, A. R. Tzafriri, and M. Socolovsky. 2012. 'Stat5 signaling specifies basal versus stress erythropoietic responses through distinct binary and graded dynamic modalities', *PLoS Biol*, 10: e1001383.

Rapetti-Mauss, R., C. Lacoste, V. Picard, C. Guitton, E. Lombard, M. Loosveld, V. Nivaggioni, N. Dasilva, D. Salgado, J. P. Desvignes, C. Beroud, P. Viout, M. Bernard, O. Soriani, H. Vinti, V. Lacroze, M. Feneant-Thibault, I. Thuret, H. Guizouarn, and C. Badens. 2015. 'A mutation in the Gardos channel is associated with hereditary xerocytosis', *Blood*, 126: 1273-80.

Rapetti-Mauss, R., V. Picard, C. Guitton, K. Ghazal, V. Proulle, C. Badens, O. Soriani, L. Garcon, and H. Guizouarn. 2017. 'Red blood cell Gardos channel (KCNN4): the essential determinant of erythrocyte dehydration in hereditary xerocytosis', *Haematologica*, 102: e415-e18.

Rets, A., A. L. Clayton, R. D. Christensen, and A. M. Agarwal. 2019. 'Molecular diagnostic update in hereditary hemolytic anemia and neonatal hyperbilirubinemia', *Int J Lab Hematol*, 41 Suppl 1: 95-101.

Rivera, A., D. H. Vandorpe, B. E. Shmukler, D. R. Gallagher, C. C. Fikry, F. A. Kuypers, C. Brugnara, L. M. Snyder, and S. L. Alper. 2017. 'Erythrocytes from hereditary xerocytosis patients heterozygous for KCNN4 V282M exhibit increased spontaneous Gardos channel-like activity inhibited by senicapoc', *Am J Hematol*, 92: E108-E10.

Russo, R., I. Andolfo, F. Manna, G. De Rosa, L. De Falco, A. Gambale, M. Bruno, A. Matte, P. Ricchi, D. Girelli, L. De Franceschi, and A. Iolascon. 2016. 'Increased levels of ERFE-encoding FAM132B in patients with congenital dyserythropoietic anemia type II', *Blood*, 128: 1899-902.

Russo, R., I. Andolfo, F. Manna, A. Gambale, R. Marra, B. E. Rosato, P. Caforio, V. Pinto, P. Pignataro, K. Radhakrishnan, S. Unal, G. Tomaiuolo, G. L. Forni, and A. Iolascon. 2018. 'Multi-gene panel testing improves diagnosis and management of patients with hereditary anemias', *Am J Hematol*, 93: 672-82.

Russo, R., M. R. Esposito, and A. Iolascon. 2013. 'Inherited hematological disorders due to defects in coat protein (COP)II complex', *Am J Hematol*, 88: 135-40.

Russo, R., A. Gambale, C. Langella, I. Andolfo, S. Unal, and A. Iolascon. 2014. 'Retrospective cohort study of 205 cases with congenital dyserythropoietic anemia type II: definition of clinical and molecular spectrum and identification of new diagnostic scores', *Am J Hematol*, 89: E169-75.

Russo, R., C. Langella, M. R. Esposito, A. Gambale, F. Vitiello, F. Vallefuoco, T. Ek, E. Yang, and A. Iolascon. 2013. 'Hypomorphic mutations of SEC23B gene account for mild phenotypes of congenital dyserythropoietic anemia type II', *Blood Cells Mol Dis*, 51: 17-21.

Russo, R., R. Marra, B. E. Rosato, A. Iolascon, and I. Andolfo. 2020. 'Genetics and Genomics Approaches for Diagnosis and Research Into Hereditary Anemias', *Front Physiol*, 11: 613559.

Salzberger, W., W. F. Garcia-Beltran, H. Dugan, S. Gubbala, C. Simoneau, S. B. Gressens, S. Jost, and M. Altfeld. 2015. 'Influence of Glycosylation Inhibition on the Binding of KIR3DL1 to HLA-B*57:01', *PLoS One*, 10: e0145324.

Sangkhae, V., and E. Nemeth. 2019. 'To induce or not to induce: the fight over hepcidin regulation', *Haematologica*, 104: 1093-95.

Schmidt, P. J., N. C. Andrews, and M. D. Fleming. 2010. 'Hepcidin induction by transgenic overexpression of Hfe does not require the Hfe cytoplasmic tail, but does require hemojuvelin', *Blood*, 116: 5679-87.

Schwarz, K., A. Iolascon, F. Verissimo, N. S. Trede, W. Horsley, W. Chen, B. H. Paw, K. P. Hopfner, K. Holzmann, R. Russo, M. R. Esposito, D. Spano, L. De Falco, K. Heinrich, B. Joggerst, M. T. Rojewski, S. Perrotta, J. Denecke, U. Pannicke, J. Delaunay, R. Pepperkok, and H. Heimpel. 2009. 'Mutations affecting the secretory COPII coat component SEC23B cause congenital dyserythropoietic anemia type II', *Nat Genet*, 41: 936-40.

Shmukler, B. E., D. H. Vandorpe, A. Rivera, M. Auerbach, C. Brugnara, and S. L. Alper. 2014. 'Dehydrated stomatocytic anemia due to the heterozygous mutation R2456H in the mechanosensitive cation channel PIEZO1: a case report', *Blood Cells Mol Dis*, 52: 53-4.

Shokrgozar, N., and H. A. Golafshan. 2019. 'Molecular perspective of iron uptake, related diseases, and treatments', *Blood Res*, 54: 10-16.

Silvestri, L., F. Guillem, A. Pagani, A. Nai, C. Oudin, M. Silva, F. Toutain, C. Kannengiesser, C. Beaumont, C. Camaschella, and B. Grandchamp. 2009.

'Molecular mechanisms of the defective hepcidin inhibition in TMPRSS6 mutations associated with iron-refractory iron deficiency anemia', *Blood*, 113: 5605-8.

Silvestri, L., A. Nai, A. Dulja, and A. Pagani. 2019. 'Hepcidin and the BMP-SMAD pathway: An unexpected liaison', *Vitam Horm*, 110: 71-99.

Silvestri, L., A. Pagani, A. Nai, I. De Domenico, J. Kaplan, and C. Camaschella. 2008. 'The serine protease matriptase-2 (TMPRSS6) inhibits hepcidin activation by cleaving membrane hemojuvelin', *Cell Metab*, 8: 502-11.

Skop, A. R., H. Liu, J. Yates, 3rd, B. J. Meyer, and R. Heald. 2004. 'Dissection of the mammalian midbody proteome reveals conserved cytokinesis mechanisms', *Science*, 305: 61-6.

Stadtman, E. R. 1992. 'Protein oxidation and aging', *Science*, 257: 1220-4.

Sugimoto, A., A. Miyazaki, K. Kawarabayashi, M. Shono, Y. Akazawa, T. Hasegawa, K. Ueda-Yamaguchi, T. Kitamura, K. Yoshizaki, S. Fukumoto, and T. Iwamoto. 2017. 'Piezo type mechanosensitive ion channel component 1 functions as a regulator of the cell fate determination of mesenchymal stem cells', *Sci Rep*, 7: 17696.

Syeda, R., J. Xu, A. E. Dubin, B. Coste, J. Mathur, T. Huynh, J. Matzen, J. Lao, D. C. Tully, I. H. Engels, H. M. Petrassi, A. M. Schumacher, M. Montal, M. Bandell, and A. Patapoutian. 2015. 'Chemical activation of the mechanotransduction channel Piezo1', *Elife*, 4.

Syfuss, P. Y., A. Ciupea, S. Brahimi, T. Cynober, G. W. Stewart, B. Grandchamp, C. Beaumont, G. Tchernia, J. Delaunay, and J. C. Wagner. 2006. 'Mild dehydrated hereditary stomatocytosis revealed by marked hepatosiderosis', *Clin Lab Haematol*, 28: 270-4.

Tamary, H., H. Offret, O. Dgany, B. Foliguet, S. N. Wickramasinghe, T. Krasnov, F. Rumilly, C. Goujard, M. Feneant-Thibault, T. Cynober, and J. Delaunay. 2008. 'Congenital dyserythropoietic anaemia, type I, in a

Caucasian patient with retinal angioid streaks (homozygous Arg1042Trp mutation in codanin-1)', *Eur J Haematol*, 80: 271-4.

Tanno, T., N. V. Bhanu, P. A. Oneal, S. H. Goh, P. Staker, Y. T. Lee, J. W. Moroney, C. H. Reed, N. L. Luban, R. H. Wang, T. E. Eling, R. Childs, T. Ganz, S. F. Leitman, S. Fucharoen, and J. L. Miller. 2007. 'High levels of GDF15 in thalassemia suppress expression of the iron regulatory protein hepcidin', *Nat Med*, 13: 1096-101.

Tao, J., M. Zhu, H. Wang, S. Afelik, M. P. Vasievich, X. W. Chen, G. Zhu, J. Jensen, D. Ginsburg, and B. Zhang. 2012. 'SEC23B is required for the maintenance of murine professional secretory tissues', *Proc Natl Acad Sci U S A*, 109: E2001-9.

Utsugisawa, T., J. L. Moody, M. Aspling, E. Nilsson, L. Carlsson, and S. Karlsson. 2006. 'A road map toward defining the role of Smad signaling in hematopoietic stem cells', *Stem Cells*, 24: 1128-36.

von Lindern, M., M. Parren-van Amelsvoort, T. van Dijk, E. Deiner, E. van den Akker, S. van Emst-de Vries, P. Willems, H. Beug, and B. Lowenberg. 2000. 'Protein kinase C alpha controls erythropoietin receptor signaling', *J Biol Chem*, 275: 34719-27.

Wallace, D. F., L. Summerville, E. M. Crampton, D. M. Frazer, G. J. Anderson, and V. N. Subramaniam. 2009. 'Combined deletion of Hfe and transferrin receptor 2 in mice leads to marked dysregulation of hepcidin and iron overload', *Hepatology*, 50: 1992-2000.

Wang, C. Y., and J. L. Babitt. 2019. 'Liver iron sensing and body iron homeostasis', *Blood*, 133: 18-29.

Wang, C. Y., A. B. Core, S. Canali, K. B. Zumbrennen-Bullough, S. Ozer, L. Umans, A. Zwijsen, and J. L. Babitt. 2017. 'Smad1/5 is required for erythropoietin-mediated suppression of hepcidin in mice', *Blood*, 130: 73-83.

Zaninoni, A., E. Fermo, C. Vercellati, D. Consonni, A. P. Marcello, A. Zanella, A. Cortelezzi, W. Barcellini, and P. Bianchi. 2018. 'Use of Laser Assisted Optical Rotational Cell Analyzer (LoRRca MaxSis) in the Diagnosis

of RBC Membrane Disorders, Enzyme Defects, and Congenital Dyserythropoietic Anemias: A Monocentric Study on 202 Patients', *Front Physiol*, 9: 451.

Zarychanski, R., V. P. Schulz, B. L. Houston, Y. Maksimova, D. S. Houston, B. Smith, J. Rinehart, and P. G. Gallagher. 2012. 'Mutations in the mechanotransduction protein PIEZO1 are associated with hereditary xerocytosis', *Blood*, 120: 1908-15.

Zhao, N., and C. A. Enns. 2013. 'N-linked glycosylation is required for transferrin-induced stabilization of transferrin receptor 2, but not for transferrin binding or trafficking to the cell surface', *Biochemistry*, 52: 3310-9.